The plasma discharge mechanism in wire chambers in the regime of large gas gain

B. Zh. Zalikhanov
Joint Institute for Nuclear Research, Dubna

Fiz. Élem. Chastits At. Yadra **29**, 1194–1258 (September–October 1998)

The results of studies of wire chambers with gas gain corresponding to streamer production in the electron avalanche are reviewed. The dynamics of the development of an avalanche and its transformation into plasma production are demonstrated experimentally for the first time. Some qualitatively new features appear which allow the determination of the necessary conditions for streamer formation and growth toward the cathode. The results of these studies can be used to develop techniques for physics experiments and in gas-discharge physics.
 [S1063-7796(98)00405-7]

1. INTRODUCTION

It follows from the classification of the various types and regions of gas discharge in nonuniform electric fields that Townsend discharge evolves into either corona discharge (the Geiger–Müller regime) or self-quenching streamer discharge. The regime into which the discharge evolves depends both on the composition of the gas in which the discharge occurs, and on the geometrical parameters of the chamber.[1–4]

It is well known that for the transformation of Townsend discharge into corona discharge, the decisive role in shower development is played by photoionization. Here the total gas gain factor, given by[5]

$$M_\gamma = M + M^2\gamma + M^3\gamma^2 + \ldots = \frac{M}{1-M_\gamma}, \qquad (1)$$

can significantly exceed the gas gain factor M of a Townsend avalanche, because the probability γ for the appearance of a photoelectron per secondary electron grows with increasing voltage.

For larger concentration of quench impurities and higher voltage, Townsend discharge becomes self-quenching streamer discharge. In contrast to streamer discharge in a uniform field, a streamer formed in a nonuniform field near the anode wire, in moving toward the cathode, reaches regions with low electric-field strength and ceases to exist. We can give only a qualitative picture of the mechanism of evolution of a Townsend avalanche into streamer discharge in a nonuniform field, based mainly on the streamer theory proposed by Loeb and Meek for a uniform electric field.[6] It is assumed that here, as in the Geiger–Müller region, the decisive role in the creation of secondary avalanches is played by photons produced in the development of the primary avalanche and capable of ionizing the gas molecules. If the electric field of the avalanche has about the same magnitude as the external field, the superposition of the two gives a field which is much stronger on the avalanche axis than off to the side of it. Therefore, there will be preferential development of avalanches near the primary avalanche axis. These secondary avalanches will affect the primary one and produce a streamer.[7]

So far there has been no experimental confirmation of this mechanism for either uniform or nonuniform electric fields, and strong doubts remain. The fact of ionization of a gas by the short-wavelength radiation of an avalanche with the number of charge carriers close to the critical value ($N_{cr} \approx 10^8$) has been recorded by Raether.[8] Subsequent studies of photoionization by light from an avalanche[9,10] have shown that short-wavelength radiation is characterized by very high absorption coefficient $\mu = (200–600)$ cm^{-1} and relatively low photon yield per secondary electron ($N_{ph} \leqslant 10^{-3}$ for $E/p \leqslant 100$ V/cm·Torr). As the gas pressure increases, N_{ph} decreases, owing to quenching of the excited atoms and molecules.[11] Obviously, these values for the yield of ionizing radiation from a discharge and its absorption in a gas do not favor the photoionization mechanism. To create secondary electrons, the photons must pass from the front of the primary avalanche toward the cathode, traveling a distance at least equal to the length of the avalanche, i.e., ~ 200 μm, while their absorption length in the gas is (20–40) μm.

The high degree of localization of an avalanche near the avalanche axis in the self-quenching streamer regime, demonstrated in Ref. 12, also indicates strong suppression of the photoionization process; otherwise, before the avalanche is transformed into a streamer the photons would be more likely to produce secondary electrons along the anode wire, because this requires two to three times smaller mean free path. The possibility of this mechanism was indicated by the results of a study of the characteristics of a chamber operating in the prestreamer regime.[13] It was shown that the electric field near the anode wire beyond the developing avalanche is not screened by the space charge and practically preserves its magnitude.

It is thought that, for secondary avalanches forming a streamer directed toward the cathode, bare electrons can also be created as a result of associative ionization reactions of the type $A + A^* = A_2^+ + e^-$ occurring in the avalanche tail. Ionization of this type is most efficient when the atomic

ionization potential is comparable to the dissociation energy of a molecular ion.[14] Another source of secondary avalanches might be multistage ionization in collisions of electrons with excited atoms, the number of which grows with increasing electric field in the chamber.[15] As a result, atoms or molecules are ionized by the numerous slow electrons present in a strong avalanche. This mechanism can be switched on because the cross section for ionizing excited atoms and molecules by electrons is large compared with the cross section for ionizing atoms and molecules in the ground state.[15]

There is a real possibility that these processes occur in strong avalanches with gas gain $>10^7$ (Ref. 14). However, experimental confirmation is needed before they can be regarded as sources of secondary electrons behind the avalanche front.

2. PURPOSE OF THE STUDY

The purpose of the present study is to analyze the data on the development of an electron avalanche in the region between the limited-proportional regime and the self-quenching streamer regime for various gas mixtures. The presence of a complex gas in a chamber causes the discharge to occur in only a single stage owing to ionization by electron impact, and the effect of the photon mechanism is eliminated.

This region is interesting for the following reasons. The development of an avalanche in a wire chamber takes a very small but finite time, and before the electrons have traveled to the anode the concentrations of positive and negative charge in the avalanche are practically identical. As the gas gain increases, the charge density in the avalanche grows, and, when it reaches a certain value, electrical forces between charges of opposite sign begin to manifest themselves. Since the ions and electrons in the avalanche drift in opposite directions with different velocities, the drift in the avalanche necessarily leads to charge separation and the appearance of an electric field which tends to counteract the separation. The effect of an external electric field tending to separate bound charges will be weakened considerably with increasing gain, owing to the increased screening of the charges inside the avalanche. The penetration depth of an external electric field in the region occupied by the charges is given by

$$E=E_0\cdot e^{-x/r_D}, \tag{2}$$

where E_0 is the field strength outside the avalanche, E is the field strength at a distance x from the edge of the avalanche, and r_D is the Debye radius characterizing the distances at which charge separation in the avalanche can occur with electron density n and thermal energy kT_e (T_e is the electron temperature, understood not in the strict sense, but rather as a quantity characterizing the average thermal energy of the electrons, because an avalanche in a nonuniform field cannot be in a state of thermodynamical equilibrium).

The higher the avalanche density, the smaller the scales of the charge separation in space and time, and the stronger the automatic mechanism for balancing charges of opposite sign. The motion of the particles in the avalanche is such that the ions cannot be separated from the electrons.[17] The dynamics of the avalanche development under these conditions must be qualitatively different, because the avalanche begins to be transformed into a plasma state.[18] This means that in an avalanche with gas gain 10^7-10^8 purely plasma processes such as electron bremsstrahlung, electrical neutralization of charges, electrostatic plasma oscillations of the ion branch, and other processes[17,19,20] absent in a Townsend avalanche must occur.

3. GENERAL CONSIDERATIONS

The gas-discharge phenomenon was analyzed in Ref. 21, and here it will be useful to review briefly those results and to give some additional information about discharge in wire chambers.

An electron avalanche in a multiwire chamber begins with a small number of primary ionization centers which are formed along the tracks of the recorded particles. Simultaneously with the ionization, which ensures electron multiplication under the influence of the electric field of the chamber, processes occur which inhibit avalanche development.

There are three main processes which inhibit an avalanche: electron energy losses, losses of the electrons themselves, and departure of electrons from the region of avalanche development near the anode wire owing to diffusion. The first process slows the acquisition by an electron in the electric field of the chamber of an energy sufficient for ionization. The other two processes lead to complete or partial breaking of chains in the multiplication chain reaction. The fate of an avalanche is therefore decided at an early stage, when the probability for electron loss owing to recombination with ions is still practically zero.

The energy lost by electrons in molecular gases goes mainly into excitation of vibrational and electron levels. The role played by these processes in discharge is well understood. The first serves to transfer the electron energy to the molecules and thereby raises the gas temperature. The second leads to excitation of the molecules, which can then be ionized by the many relatively slow electrons present in an intense avalanche. In the end, these processes tend to slow down the avalanche development. Therefore, to obtain a large gas gain and speed up the avalanche development in a molecular gas, it is necessary that the gas possess sufficient dielectric strength in order to support high values of the electric-field strength. For a suitable choice of working gas, the electric field near the anode in wire chambers can reach values of $(3-5)\times10^5$ V/cm with strong nonuniformities. Over the electron mean free path ($l\approx10^{-4}$ cm) the field can vary by up to 10% along the direction toward the anode. For this reason, an electron moving near the anode cannot acquire the equilibrium velocity corresponding to a given value of the field, i.e., the electron cannot manage to transform the energy obtained from the field into energy of random motion. Consequently, some of the electrons in the avalanche in a region where the electric field is strongly nonuniform pass into the acceleration regime, and the growing ionization intensity is shifted in the direction of the motion.[22] The transition of some of the electrons into the acceleration regime

strongly weakens the bremsstrahlung effect of the ions on them owing to the rapid falloff of the Coulomb interaction.[17]

The electron loss in an avalanche can to some degree be influenced by choosing a gas mixture which does not contain an electrically negative component. If the gas does contain such a component, "quenching" additives are used to "cool down" the electrons by decreasing their average energy in collisions with molecules of the quench gas and transferring this energy to the region of the Ramsauer–Townsend minimum in the electron scattering cross section.[15]

The departure of electrons from the avalanche-production region near the anode as a result of diffusion can be significantly decreased by enlarging this region. This can be done in two ways, namely, by making the anode plane from thick wires of diameter $\geqslant 50$ μm in chambers with an anode–cathode gap of 5–8 mm (Ref. 4), or by decreasing the anode–cathode gap and the spacing of the signal wires to 1–2 mm. In this case the anode plane can be made of wires of diameter 10–20 μm (Ref. 23). The use of anode wires of diameter $\geqslant 50$ μm in narrow-gap chambers significantly enlarges the avalanche-production region, but then the pulse amplitude becomes strongly dependent on the point of incidence and direction of motion of the recorded particles.[13]

Therefore, in both narrow-gap chambers and standard chambers with thick anode wire, when a suitable gas mixture is used a very high gas gain [of order $(5-10)\times 10^7$; Refs. 13, 24, and 28] can be attained, and the well known Loeb and Meek breakdown condition[6] $\alpha(E_0)d=18-19$ is reached for a uniform electric field of strength E_0. Here d is the inter-electrode spacing, and α is the ionization coefficient. According to the theory of Loeb and Meek, when this condition is satisfied a streamer is produced. In narrow-gap chambers with small spacing of the anode wires, the value of E/p averaged along the lines of force is considerably higher than in standard chambers. This is the reason why narrow-gap chambers are a good tool for obtaining information about the avalanche development at the instant when a streamer is formed.

4. THE EXPERIMENTAL APPARATUS

Data on the development of an electron avalanche in the region between the limited-proportional and self-quenching streamer regimes have been obtained by using two narrow-gap chambers with the following geometry:

Chamber 1: Signal-wire spacing 1.1 mm; anode–cathode separation ± 1.5 mm; sensitive area 150×140.8 mm^2; number of anode wires 128.

Chamber 2: Anode-wire spacing 2.2 mm; anode–cathode separation ± 2 mm; sensitive area 220×211.2 mm^2; number of anode wires 96.

The anode wire in the chambers was made of gold-plated tungsten and had diameter 20 μm; it was manufactured by Luma Metals.[25] The cathodes were made of Lavsan film with a carbon coating. The thickness of the Lavsan was 20 μm, and the carbon coating was 5 μm thick. The resistivity of the conducting layer of the cathodes was 400 Ω/cm^2. The chambers were made using the technology described in Ref. 26.

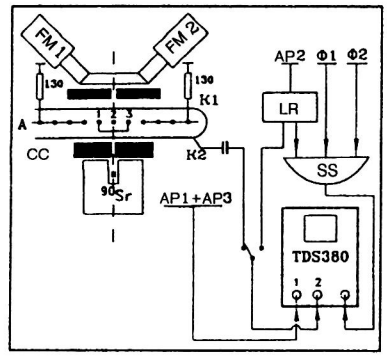

FIG. 1. Scheme for measuring the chamber characteristics and an electron avalanche.

The measurements were performed at a stand (Fig. 1) using the radioactive sources ^{90}Sr and ^{55}Fe. The passage of β particles through the chamber was recorded by a scintillation detector scanned from the faces by two photomultipliers connected in coincidence. The signals from the coincidence circuit were used to control the charge-code block when analyzing the amplitude characteristics and as the start signal when measuring the time characteristics of the chambers.

The electron beam and its intensity were shaped by means of regulated gap collimators located in front of the chamber and right at the scintillation counter. The recording of electrons scattered on the chamber material was partially suppressed by varying the width of the gap collimators and the distance between them and the chamber.

The chambers were filled with the gas mixture 80% CF_4+20% C_4H_{10}.

The 32-channel preamplifiers for the signal electrodes were based on the MAR6 solid-state amplifier manufactured by MiniCircuits[27] and placed directly on the chamber. When measuring the signal amplitude, the output of one of the preamplifier channels was sent (for low gain in the chamber) to the input of the second amplifier with a gain factor of 10, and then to the input of the charge–code block. In these measurements the gap collimators were tuned to the selected channel. When measuring the time jitter, the signals from the preamplifier output were sent to two 16-channel comparator chips. After logical addition of the signals by Fast OR, the signal was sent from these chips to the stop input of the time encoder.

A high voltage was fed to the chamber cathodes via a terminating resistance equal to 3 MΩ. Information from the cathodes was unloaded via a high-voltage capacitance 220 pF×6 kV. These channels were also used to monitor the chamber and the electronics, for which square pulses of duration 10 nsec and amplitude 0.7 V were fed via them from a generator to the chamber cathodes. These pulses were sent through the anode–cathode capacitance via the signal wires to the amplifier inputs.

5. THE ELECTRIC-FIELD DISTRIBUTION IN THE CHAMBERS

The field in the chambers (Fig. 1) was determined by the method of images. The field in a chamber at the point (x,z) has the form

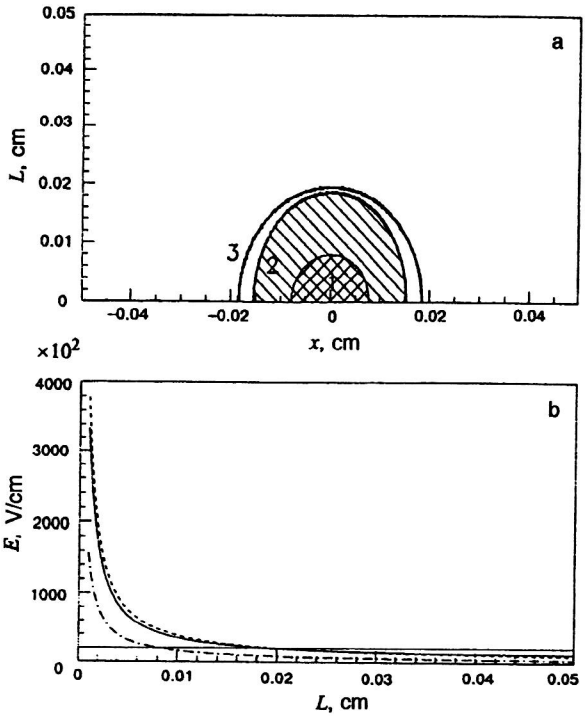

FIG. 2. (a) Region of avalanche production near the anode wire, limited to field strength 20 kV/cm, and electric-field distribution in the direction toward the cathode. (1) $L_0/2=8$, $S=2$, $d=0.02$; (2) $L_0/2=1.5$, $S=1$, $d=0.02$; (3) $L_0/2=2$, $S=2$, $d=0.02$. (b) electric-field distribution: $L_0/2=15$, $S=1$, $d=0.02$ (solid curve); $L_0/2=2$, $S=2$, $d=0.02$ (dashed curve); $L_0/2=8$, $S=1$, $d=0.02$ (dot–dash curve). The geometrical parameters of the chambers are given in mm. The chamber voltage is 2500 V.

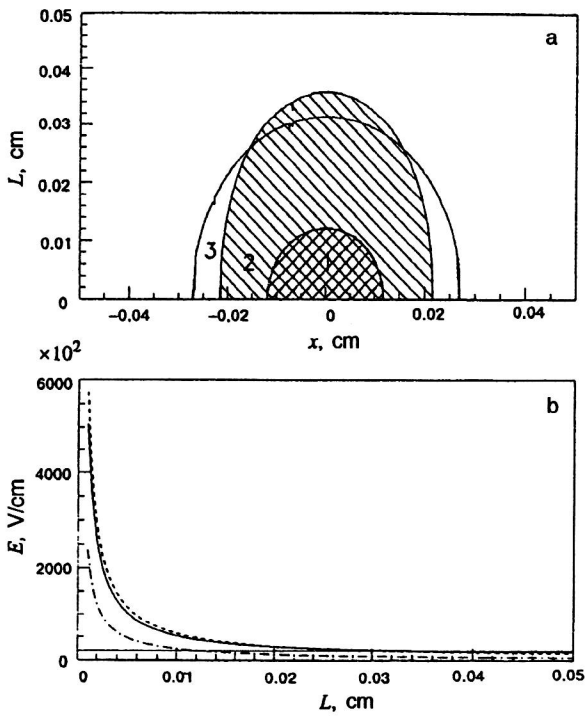

FIG. 3. The same as in Fig. 2, for chamber voltage of 3800 V.

$$E_x=\frac{2\pi U_0}{z_0 C_0}\sum_{k=-m}^{k=m}\frac{\sinh\dfrac{\pi(x-ks)}{z_0}\cos\dfrac{\pi z}{z_0}}{\cosh\dfrac{2\pi(x-ks)}{z_0}-\cos\dfrac{2\pi z}{z_0}}, \tag{3}$$

$$E_z=\frac{2\pi U_0}{z_0 C_0}\sum_{k=-m}^{k=m}\frac{\cosh\dfrac{\pi(x-ks)}{z_0}\sin\dfrac{\pi z}{z_0}}{\cosh\dfrac{2\pi(x-ks)}{z_0}-\cos\dfrac{2\pi z}{z_0}}, \tag{4}$$

$$C_0=\sum_{k=-m}^{k=m}\tanh^{-1}\left(\frac{\cos\dfrac{\pi r_0}{z_0}}{\cosh\dfrac{\pi k s}{z_0}}\right). \tag{5}$$

Here z_0 is twice the anode–cathode spacing, s is the anode-wire gap, and $2m+1$ is the number of anode wires in the chamber.

In Figs. 2a and 3a we show the electric-field distributions for chamber voltages of 2.5 kV and 3.8 kV in the z direction from the anode wire to the cathode for chambers 1 and 2, and also for a standard chamber. Calculations of the electric-field distribution showed that the value of E/p averaged over the drift path for chambers 1 and 2 was more than 5 to 8 times higher than in the standard chamber. If the threshold value for avalanche production is taken to be a field of 20 kV/cm (the ionization potential of CF_4 is 17 eV, and the electron mean free path in the gas is $\sim 10^{-3}$ cm), then for a chamber voltage of 3.8 kV this field is produced in chamber 1 at a distance $d=0.35$ mm, in chamber 2 at 0.3 mm, and in the standard chamber at 0.12 mm from the anode wire. The shape and area of the avalanche-production regions bounded by electric-field strength 20 kV/cm are illustrated in Figs. 2b and 3b. An enlarged avalanche-production region of this type (Fig. 4) is realized in the chambers with thick anode wire described in Refs. 1–4, where the characteristics of the self-quenching streamer regime were studied.

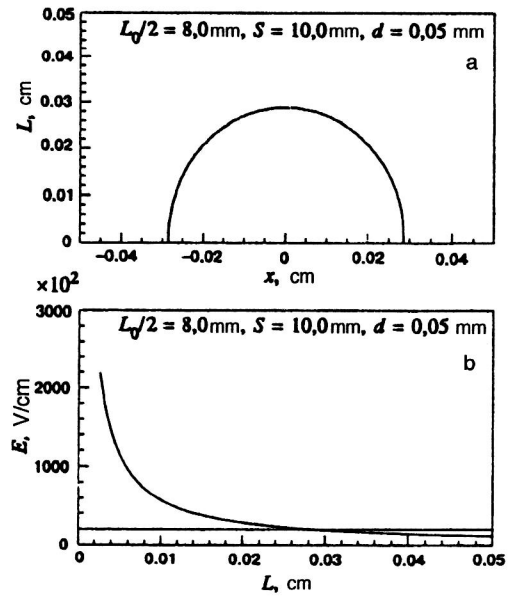

FIG. 4. The same as in Fig. 2, for a chamber with a thick wire. The chamber voltage is 3500 V.

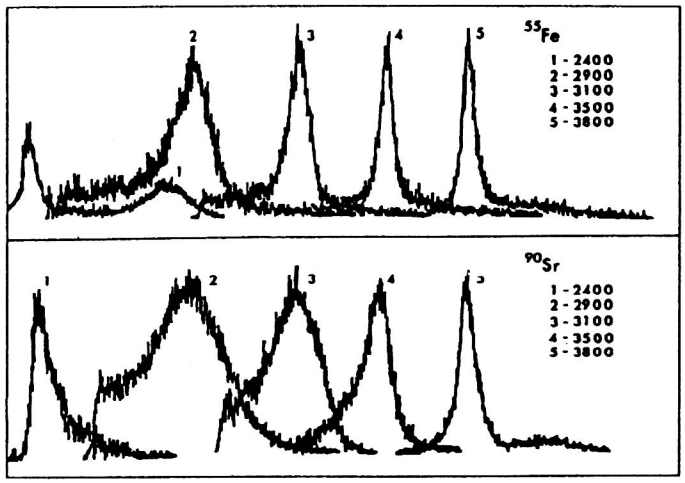

FIG. 5. Change of shape of the amplitude spectra obtained from ^{55}Fe and ^{90}Sr sources as a function of the high voltage on the chamber.

6. CHAMBER CHARACTERISTICS

Since all the characteristics measured for chambers 1 and 2 practically coincide (except for the time jitter and the speed of action), below we shall give the measurement results for chamber 1. The differences between chambers 1 and 2 will be discussed specially in Sec. 6.2 devoted to the time characteristics. The fact that the characteristics of chambers 1 and 2 are practically identical is not surprising when one compares the electric-field distributions in the chambers and the sizes of the avalanche-production regions. As can be seen from Figs. 2 and 3, these values are practically the same over the entire voltage range.

The choice of the narrow-gap chamber 1 was dictated by the following considerations. There are quite contradictory views on the operation of such chambers in the gas-gain regime ($>5\times10^6$). In a study performed at CERN,[28] it was assumed that the chamber operates in the limited streamer regime. At the same time, studies performed at the Institute of Experimental Physics, Warsaw University[29] showed that the amplitudes of signals from the chamber depend on the primary ionization. In Refs. 30 and 31, reporting on work at the TRIUMF accelerator in Canada and at the Institute of High Energy Physics at Serpukhov, it was shown that chambers of this type can operate at high counting rates, while remaining highly stable to radiation. Finally, the authors of Refs. 32 and 33 express doubt that stable operation of narrow-gap chambers with anode wire >10 μm wound with small pitch is possible in principle.

Owing to the contradictory views regarding the operation of narrow-gap chambers in the region of large gas gain, it appeared useful to make a more detailed study of the operation of the chamber in this region. This is especially true because, as noted earlier, this region is where the transformation of an avalanche into a streamer originates.

The basic features of the chambers in the region of proportional gain, 2200–2600 V, are in good agreement with the results obtained in Ref. 30 for the chamber labeled there as No. 2. Therefore, here we mainly give the results for voltages above 2600 V, which have not been adequately studied, either in Ref. 30 or in Refs. 28–32.

6.1. The amplitude characteristics

In Fig. 5 we show the amplitude spectra for β particles and γ quanta which passed through the chamber and were absorbed in the gas gap. The spectra labeled 1 were measured for a chamber voltage of 2400 V and illustrate the operation of the chamber in the proportional regime. The amplitude spectrum 1 from ^{90}Sr has the shape of a Landau distribution, while spectrum 1 from ^{55}Fe determines the energy resolution of the chamber, equal to 21% (FWHM). The proportionality in the chamber is violated with increasing voltage. The continuous variation of the shape of the amplitude spectra differs qualitatively for the two sources, but still they nearly completely coincide with each other at the end of the efficiency plateau. The amplitude spread of these spectra is 10%, and the charge gain is greater than 5×10^7. The strong saturation of the signals from the anode wires indicates stable operation of the chamber and is mainly determined by the chamber configuration, the working gas, and the high average value of E/p in the extended avalanche-production region around the anode wires.

The extended avalanche-production region is also manifested in the behavior of the pulse amplitudes when the chamber is bombarded by ^{90}Sr and ^{55}Fe sources (Fig. 6). Even for the large difference in the number of primary ion

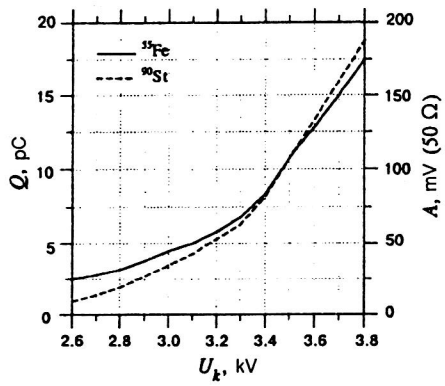

FIG. 6. Average amplitude of the signal at the anode of the chamber from the sources ^{55}Fe and ^{90}Sr as a function of the chamber voltage.

pairs produced by these sources in the chamber (a factor of about 2.2), beginning at a voltage of 3500 V the amplitude of the signals from ^{90}Sr exceeds that from ^{55}Fe. In spite of the supersaturated operating regime of the chamber at high voltages, the dependences shown in Fig. 6 tend to constant growth of the amplitude. Moreover, we see from the figure that, beginning at a voltage of 3300 V, the behavior of the gas gain undergoes an obvious qualitative change: it grows much more strongly. To obtain a clear demonstration of the degree of gas gain in the chamber, the right-hand scale in Fig. 6 corresponds to the values of the amplitudes measured directly from the signal wires, using an oscillograph with an input impedance of 50 Ω.

As is well known, the space-charge field significantly affects the avalanche development. The limit on the proportionality region in wire chambers is directly due to the presence of this charge, the effect of which grows as the avalanche grows. A high-current gas discharge always contains a large number of slow electrons formed as a result of energy loss in inelastic collisions with gas molecules, bremsstrahlung in the field of the ion cloud, and avalanches produced from following ionization clusters. Since the time scales for charge relaxation are considerably smaller than the avalanche development time, as the charge density in the avalanche increases, processes leading to charge binding due to Coulomb forces become possible. Because of this mechanism, all the slow electrons remain practically inside the ion cloud of the avalanche, which develops owing to the electrons located at its front. As a consequence, the part of the ions enclosing the slow electrons and forming something like a dipole will be screened from the anode wire by the electrons and will therefore produce a smaller polarization at the anode than at the cathode. This mechanism must therefore be manifested as a difference between the amplitude distributions measured at the anode and at the cathode with increasing gas gain.

The results of these measurements are shown in Fig. 7, where we give the value of the chamber voltage and the magnitude of the signal attenuation. We see that at low gain ($<10^5$) the pulse amplitudes at the anode and the cathode have distributions of nearly the same shape, with the average amplitude at the anode exceeding that at the cathode by a factor of 2.4. The shape of the distributions begins to change for a chamber voltage of 3300 V. This is manifested as a clear second peak in the amplitude spectrum of pulses from the cathode. The ratio of the average amplitudes determined at the first peaks is 2.2. As the chamber voltage is raised to 3800 V the amplitude of the second peak grows, and the ratio of the average amplitudes (at the first peaks) becomes 1.6. According to Ref. 3, the observed jump in the amplitude (by about a factor of two) is related to the formation in the avalanche of a streamer directed toward the cathode.

Therefore, the difference of the amplitude spectra from the anode and the cathode of the chamber, manifested with increasing gain, may indicate the complex mechanism by which the space charge inside the avalanche acts, tending to increase the electric field at the cathode end of the ion cloud. In Secs. 8.1, 8.2, and 8.3 we present additional experimental

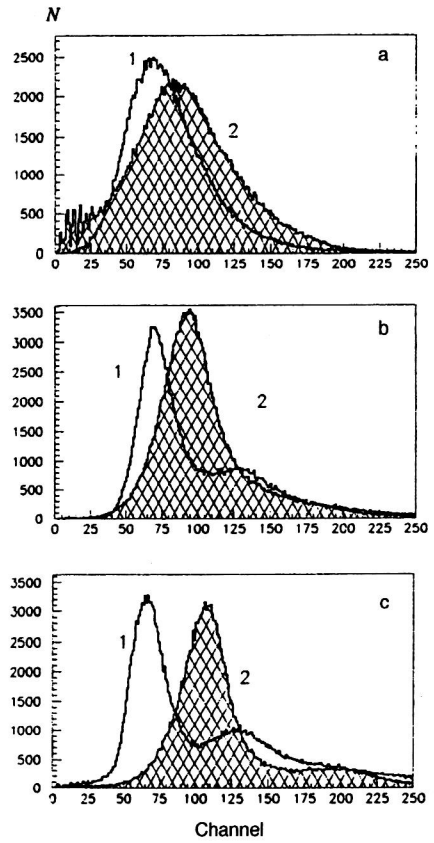

FIG. 7. (a) Amplitude distribution of signals measured at the chamber voltage 2400 V: (1) spectrum of cathode signals decreased by 6 dB; (2) spectrum of anode signals decreased by 12 dB. (b) For 3300 V: (1) spectrum of cathode signals decreased by 34 dB; (2) spectrum of anode signals decreased by 38 dB. (c) For 3800 V: (1) spectrum of cathode signals decreased by 40 dB; (2) spectrum of anode signals decreased by 40 dB.

data confirming the role of the automatic mechanism for balancing charges of opposite signs with increasing gas gain.

6.2. The time characteristics

The ratio of the drift velocity v_{dr} and the random velocity $\bar{v}$ of the electrons is given by[21]

$$\frac{v_{dr}}{\bar{v}}=\frac{\sqrt{3\pi}}{4}\sqrt{\delta}\approx 0.8\sqrt{\delta}, \tag{6}$$

where δ is the average energy loss of an electron in the gas in an individual collision event. It follows from this expression that to increase the drift velocity, it is necessary that a drifting electron, undergoing significant inelastic losses which go into excitation of the gas molecules, decrease its average energy. Cooling of drifting electrons is usually achieved in collisions with molecules of a quench gas. This process is especially efficient in strong electric fields, when over its mean free path an electron can acquire a significant energy, which it then rapidly loses to excitation of the electron states of the molecules. Here its component directed along the field increases sharply.

However, for wire chambers this trick for raising the drift velocity must involve the chamber geometry, because the addition of a quench admixture changes the average

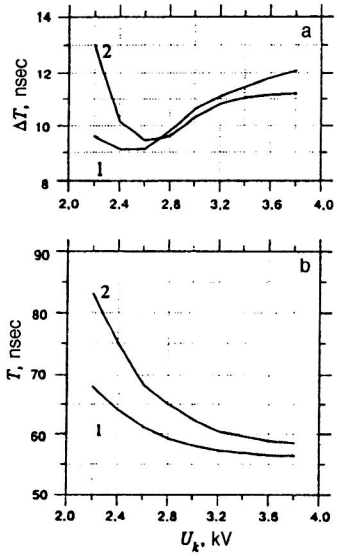

FIG. 8. Time characteristics of the chamber: (a) dependence of the time jitter on the chamber voltage for the (1) anode and (2) cathode signals; (b) change of location of the maximum in the time spectra as a function of the chamber voltage for the (1) anode and (2) cathode signals.

value of E/p. Therefore, the gas mixture must be optimized for minimum time jitter for each individual geometry.[32]

Following the recommendations of Ref. 32, the amount of isobutane added to CF_4 was optimized to obtain minimum jitter; this amount was 20%.

The variation of the time jitter for chamber 2 (FWHM) as a function of the chamber voltage is shown in Fig. 8a. A very weak decrease in the magnitude of the jitter with increasing voltage is observed for the anode signal. After the minimum value is reached, the jitter increases steadily with increasing voltage. The observed behavior of the jitter as a function of the voltage shows that, beginning at the voltage corresponding to minimum jitter, the electron drift rate in the region of large gas gain steadily decreases.[32] The analogous characteristics for chamber 1 can be found in Ref. 13.

The behavior of the jitter is somewhat different in the time analysis of the signals from the cathodes. The steeper decrease of the jitter and the shift of its minimum value to higher voltage are due to the threshold effects of the comparators, because the amplitudes of these signals are smaller than those of the anode signals by more than a factor of two. An additional reason for the shift is the large capacitance of the cathode relative to ground, which leads to integration of the signals. As the voltage increases, the jitter of the cathode signals reaches its minimum and then emerges onto a plateau.

In Fig. 8b we show the location of the average value of the time spectra for the anode (1) and cathode (2) signals as a function of the chamber voltage. The same effect, associated with the shift of the time spectra to smaller times with increasing chamber voltage, was seen in Ref. 34.

In conclusion, we note that the measured minimum jitter is completely determined by the time fluctuations of the drift of the first electrons produced near the anode plane over a length equal to half the anode spacing.[32]

The behavior of the time distributions of the signals

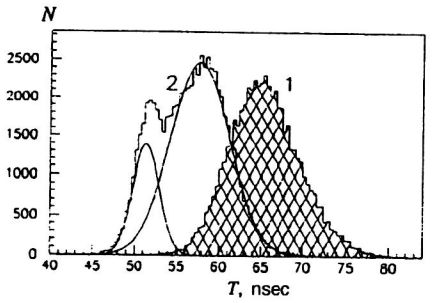

FIG. 9. Time distributions of signals from the anode of the chamber: (1) U_{ch}=2400 V; (2) U_{ch}=3700 V.

from the anode wires as a function of the chamber voltage is very striking. In Fig. 9 we show two time spectra measured at 2400 and 3700 V. Both their time displacement relative to each other and also the strong change in the shape of the distributions should be noted. Spectrum 1, obtained at 2400 V, is described well by a Gaussian distribution and indicates that the electron velocity distribution approaches a Maxwell distribution. Spectrum 2, obtained at 3700 V, explicitly disagrees with the Maxwell distribution and indicates the presence in the avalanche of at least two groups of electrons: fast and slow ones. The velocity separation of the electron avalanches begins to be manifested in the time spectra at a voltage of 2700 V (Fig. 10) and becomes stronger with increasing voltage. The difference between the average values (Fig. 9) for spectrum 1 and the slow electrons of spectrum 2 is 8 nsec, while for the fast electrons it is 12 nsec. The fact that the fast electrons run ahead of the bulk of the electrons in the avalanche by more than 7 nsec (Fig. 9) implies that the drift velocity of the slow electrons in the avalanche-production region falls. The observed increase of the time jitter in the region of large gain (Fig. 8a) is due to the constant growth of the time interval between the slow and fast electrons with increasing chamber voltage. The shift of the time spectra (Figs. 8b and 9) with increasing chamber voltage cannot be attributed to an increase of the electron drift velocity, because the magnitude of the jitter must then decrease. In fact, the jitter is observed to do the opposite (Fig. 8). The reason for this dependence is related to the avalanche development process and will be explained in Sec. 8.2. The fraction of fast showers contained in spectrum 2 can be determined if the spectrum is represented as the sum of two spectra described by Gaussian distributions. This is shown in Fig. 9, from

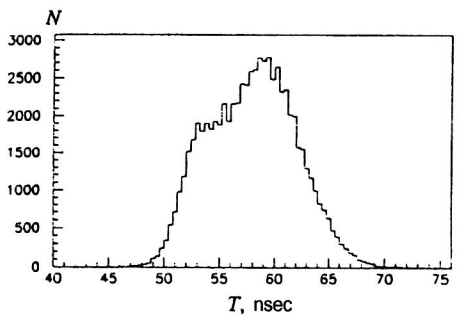

FIG. 10. Time spectrum of signals from the anode of the chamber for U_{ch} =3100 V.

which it follows that the fraction of fast electron avalanches is 31% at a voltage of 3700 V. It should be noted that the time distributions of signals from the cathode are similar to those of signals from the anode of the chamber.

As the gas gain increases, a gradual decrease in the duration of the anode signals is observed. Whereas in the proportional regime the duration of the anode signals at about 0.1 of the amplitude maximum is roughly equal to 20–40 nsec, in the high-current regime the signal duration is decreased to 5–10 nsec. The shape of the shortened signals completely mimics that of the signal shown in Fig. 8 of Ref. 28.

6.3. The counting characteristics

Bench tests of the chambers using the radioactive source ^{90}Sr were conducted for a detection threshold of 1 μA. The working efficiency plateau was 1600 V and was located in the range 2200–3800 V. The detection efficiency was 99%. At low voltages, amplifiers with a gain factor of 500 were used; these were specially designed for chamber operation at large loads. At gains of 10^6 these amplifiers were replaced by others with a gain factor of 10. For a detection threshold of 5 μA, the working plateau was located in the range 2200–3800 V for chamber 1 and 2100–3900 V for chamber 2.

The detection efficiency measured in a muon beam of intensity 10^5 sec^{-1} at an amplifier–shaper triggering threshold of 1.5 μA was 99.6% (Ref. 23). The chamber noise was measured while the accelerator was shut down. For a voltage of 2900 V, the noise from the chamber was 1 Hz per wire. At the end of the plateau the noise per wire was less than 10 Hz. This attractive feature can be attributed to the good design of the chamber, where there is no dielectric between the anode and cathodes. This eliminates the possible accumulation of electric charge in the dielectric, which could flow to the electrodes and represent the leading source of noise signals.

Study of the load characteristics of the chambers showed that there is no loss of efficiency for beam densities of up to the maximum attainable value (2.3×10^6 sec^{-1} cm^{-2}) at channel 4A of the U-70 accelerator.[23]

The chamber efficiency for gas gain in the range 10^6–10^7 decreases from 99% to 97% and is practically unchanged up to loads of 10^5 sec^{-1} cm^{-2}. Change of the detection threshold to 50 μA also does not lead to loss of efficiency.

All the amplitude, time, and counting characteristics listed above are very stable in time. Testing of the chambers at the voltage corresponding to the end of the plateau (3800 V) over a long period of time did not lead to spark breakdown. Over time, as the chamber aged owing to the high gas gain, we observed a decrease of the signal amplitude by 20% on the average in the creation at the wires of a total charge with linear density 0.5 C/cm. In further operation, no changes in the chamber were observed up to charges of 5–6 C/cm. This behavior of the chamber corresponds nearly completely to that described for chamber No. 2 in Ref. 30.

The basic characteristics of the high-current regime listed above raise a number of questions. The most important ones are the following:

1. What is the nature of the gas-discharge mechanism allowing a gain of the electron avalanche of up to $(5-10)\times10^7$ to be obtained?

2. What is the reason for the shortening of the signal duration to 5–10 nsec at about 0.1 of the amplitude maximum?

3. Why is the efficiency of the chamber operation for a gas gain of 10^7 preserved up to a beam density of 10^5 sec^{-1} cm^{-2}?

4. What is the reason for the observed constant decrease in the time of flight of the electrons at the front of the avalanche to the anode with increasing chamber voltage?

5. What causes the change of the electron velocity distribution, manifested as gaps in the time spectra at high gas gain?

None of the presently known gas-discharge mechanisms can completely answer these questions.

If, like the authors of Ref. 28, we assume that with increasing chamber voltage the gas discharge goes smoothly into the self-quenching streamer regime, then large current pulses are obtained. However, this mechanism does not explain the other observations, in particular, it does not explain the shortened signal duration and the high speed of response, which is more than two orders of magnitude greater than the speed of a chamber operating in the self-quenching streamer regime.[35]

If the Townsend avalanche mechanism forms the basis of the high-current regime,[11] then it is unclear why, with increasing gas gain, we observe not an increase of the electron time of flight to the anode owing to the bremsstrahlung effect of the space charge,[11] but a decrease of this time and a simultaneous change in the electron velocity distribution (see Figs. 9 and 10, and also Fig. 5 in Ref. 34).

Regarding the last two questions listed above, some hints at the answers can be found in Refs. 21, and 36–38, which suggest that, beginning at a certain number of charge carriers in an avalanche ($\simeq10^8$), the space-charge field creates the conditions for the continuous acceleration of the electrons moving at the front of the avalanche. This becomes possible because these electrons are screened from the positive charge by the slow electrons located behind the front, which cannot be stripped from the ions. It is for this reason that the balance between the accelerating action of the electric field, enhanced by the electrons themselves, and the decelerating collisions between the electrons and neutral particles of the gas is spoiled for the front electrons in the acceleration regime, leading to change of the electron velocity distribution.

Regarding this explanation, it should be noted that in the present study the acceleration effect and the change of the electron velocity distribution begin to be manifested when the number of charge carriers in the avalanche is 10^7, which is considerably lower than the values at which an electron avalanche becomes a streamer. The presence of such effects for a small number of particles in the avalanche requires additional explanation.

7. MEASUREMENT OF THE AVALANCHE CHARACTERISTICS BY THE OSCILLOGRAPH METHOD

Owing to the importance of understanding how an avalanche is transformed into a streamer, we studied the transition region in greater detail. As far as we know, discharges in nonuniform fields have not previously been studied by using the signals induced at many electrodes of the chamber by the charge of the avalanche at the anode wire.

To obtain more detailed information about the time development of an electron avalanche, we used the measurement scheme shown in Fig. 1. In the logic of isolating an event corresponding to the passage of an electron through the chamber, we used a single anode wire 2 connected in coincidence with a scintillation counter. The synchronizing signal for the oscillograph was triggered by the coincidence scheme when a signal arrived from the anode wire 2. This allowed the location of the analyzed signals from the chamber to be fixed on the scan of the oscillograph. The induced signals from the connected anode wires 1 and 3 (which will henceforth be referred to as the control wires) and from the connected cathode planes, and the anode signal from wire 2 were analyzed. The signals from the control wires were measured simultaneously either with the cathode or with the anode signals. The cathode and anode signals were decreased by 20 dB directly before the input to the oscillograph. All the signals were sent directly from the measured channels to the oscillograph via coaxial cables with wave impedance 50 Ω matched at both ends. The times for signal propagation from the cathode and the anode wires to the oscillograph were equalized to within $\pm 0.2\%$ and were (50 ± 0.1) nsec. The measurements were performed with a Tektronix digital two-channel oscillograph, model TDS 380 (digitizing frequency 2 GHz).

The goal of the measurements was to obtain data on the times at which the analyzed signals appear relative to each other, and also to observe the variation of the time and amplitude characteristics of the signals with increasing chamber voltage.

The measurements were performed for six different gas mixtures filling the chamber. The gas mixtures were prepared in various proportions and combinations, using rotameters, from the following assortment of gases: CF_4, C_4H_{10}, Ar, and acetone, isopropyl alcohol, and mercury vapor saturated at 25 °C. The gas purity corresponded to industrial standards and was 99.7% for CF_4, 99.997% for Ar, and 99.99% for C_4H_{10}. In each series of measurements corresponding to a particular gas filling, the minimum chamber voltage was determined by the possibility of observing signals directly from the control wires for an oscillograph sensitivity of 2 mV/division. The results of the measurements are shown in Figs. 11–14. The oscillograms in these figures were obtained by averaging 256 events. The shapes of single events were practically the same as those of the signals obtained by averaging. The signals differ only in their amplitudes, whose distribution is associated with the fluctuations in the observed processes.

The oscillograms shown on the left-hand side contain information about the development of the electron avalanche and the analyzed signals in a range of 100 nsec, while those on the right-hand side are for the first 30 nsec of this range. The different time scales allow observation of the amplitude and time characteristics of the signals, and also the change of the signal shape with varying gas gain. On the other hand, this allows more accurate monitoring and measurement of the times, at which the signals appear relative to each other. The amplitudes of the analyzed signals measured for a load of 50 Ω are plotted along the vertical axis in millivolts. Owing to the difference between the values of the amplitudes from the cathode and the anode, the vertical scales for these quantities are different in some cases. For each series of oscillograms we give the gas composition and the value of the high voltage at which they were obtained.

8. RESULTS OF THE MEASUREMENTS AND DISCUSSION

In Figs. 11–14 we show oscillograms illustrating practically all the characteristics of avalanche development, together with their dependence on the operating regime of the chamber.

8.1. Time correlation of the signals

From the oscillograms in Figs. 11–14 we see clearly that when the chamber operates with small gas gain (up to 10^5), all the analyzed signals are induced at the corresponding electrodes practically simultaneously. As the gas gain increases this correlation is spoiled, and, beginning at a gain of 10^5, the signal at the cathode begins to appear with a delay relative to the time at which the signals appear at the other electrodes. For example, when the chamber operates with a gas filling of 80% CF_4+20% C_4H_{10} (Figs. 11a–11c), the delay of the cathode signal is actually manifested when the chamber operates in the proportional regime ($V = 2300$ V). We see that the magnitude of the delay depends strongly on the chamber voltage. The maximum delay is attained for a voltage of 2600 V and is equal to the time for the amplitude of the first peak on the control wires to rise to its maximum value. The delay does not change for chamber voltages $\geqslant 2600$ V. A similar dependence holds to some degree for the other gas mixtures. A strong deviation in the behavior of the cathode-signal delay is observed when the chamber is filled with the gas mixtures 95% CF_4+5% C_4H_{10} and 70% Ar+30% C_4H_{10}. For the first of these (Figs. 11d and 11e) the delay is manifested only at the voltage 3100 V, while at 3200 V the delay is only 2.3 nsec, even though at these voltages the chamber operates in the limited-proportional regime with gain $>10^6$. For the second gas mixture (Fig. 12) there is practically no delay of the cathode signal.

Comparing the times at which signals appear at the anode and at the control wires, we see that in the entire range of high voltages the signals are formed simultaneously in the chamber.

The observed regularity in the appearance of the signal at the cathode can be explained as follows. For chamber voltages corresponding to gas gain $<10^5$, the avalanche still

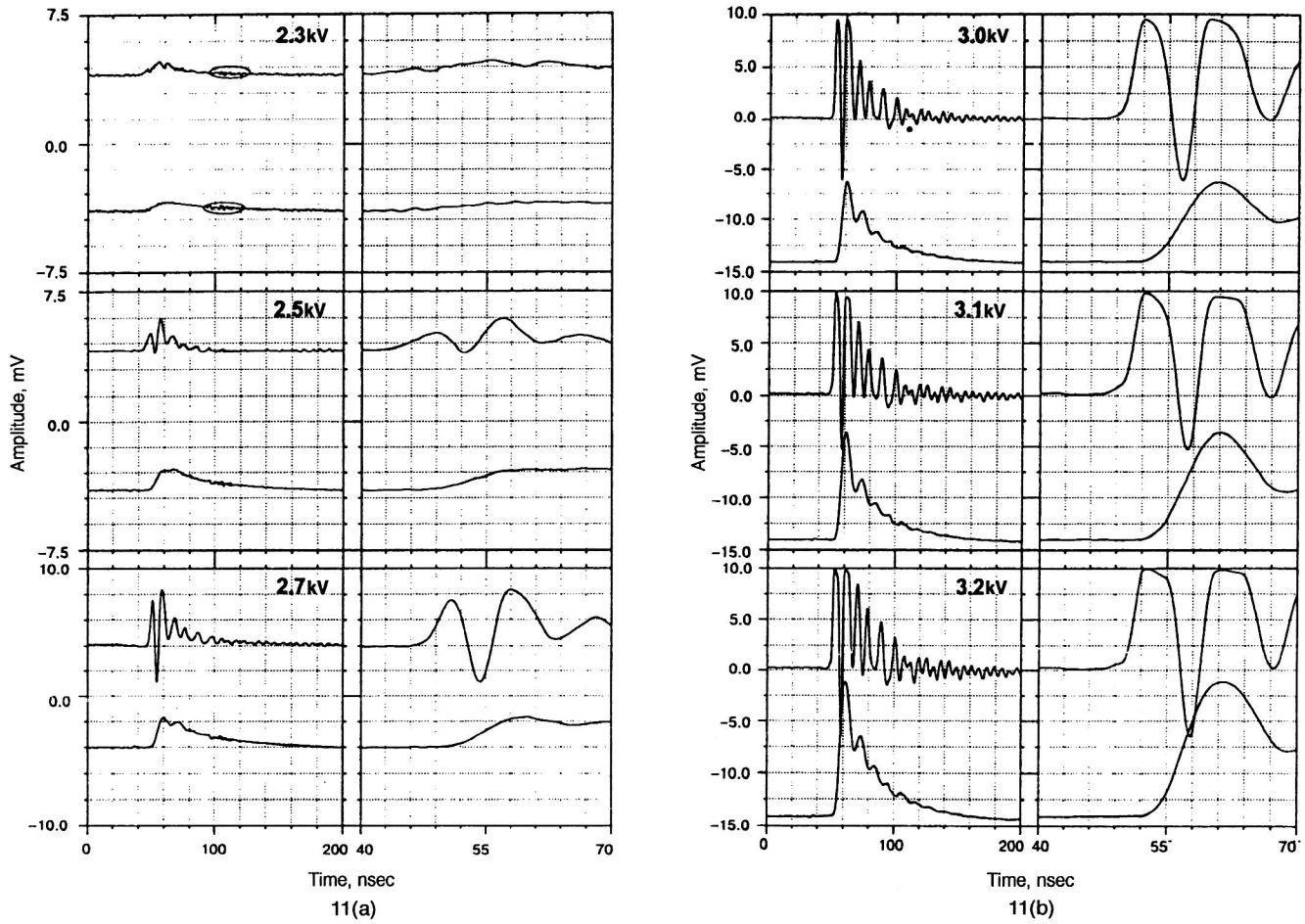

FIG. 11. Oscillograms of signals from the control wires (upper figures) and from the cathode (a–d) or anode (e) for chamber filled with the gas mixture 80% CF_4+20% C_4H_{10} (a,b,c) or 95% CF_4+5%C_4H_{10} (d,e). The chamber voltage is given on the oscillograms. The cathode signals (lower oscillograms) are decreased by 20 dB (a,b,c) and 10 dB (d), and the anode signals (e) by 12 dB.

has low charged-particle densities n_+ and n_-, and so the interaction of the charged particles in the avalanche is negligible and charges of different signs drift freely to the corresponding electrodes independently of each other. The flow of charges in a loop starts a current which is the sum of the electron and ion currents:[39]

$$i=i_+ + i_- = \frac{E}{V}(n_+ v_{dr}^+ + n_- v_{dr}^-). \qquad (7)$$

The ratio of the electric-field strength E to the potential difference V applied to the chamber is determined by the chamber geometry. In the present case, signals of the corresponding polarity are induced simultaneously at the chamber electrodes under the influence of the moving charges of the avalanche. The appearance of a delay in the signal induction at the cathode implies that the ion drift velocity v_{dr}^+ is practically zero during this time. For low avalanche density this can occur only when the ions in the avalanche tail enclosing the electrons undergo a strong mutual deceleration and simultaneously screen the cathode from the electrons moving to the anode.

However, this is not the only process in an avalanche leading to ion deceleration. In a high-current avalanche the effective drift velocity of the ions can be decreased in collisions with excited molecules and also in charge-exchange processes.[22] The directional motion of the ions in an electric field can also be spoiled in collisions with gas molecules. It is clear that these processes can affect the avalanche development only at high densities, when the number of charge carriers in the avalanche is close to the critical value of 10^8 (Ref. 38). When the avalanche has low density, the ions can be decelerated only when ambipolar diffusion is involved in the avalanche development[40] owing to the action of the Coulomb forces, which cause the binding of charges of opposite signs. The main consequence of the inclusion of this process is that the avalanche electrons begin to decelerate, and the self-consistent field of the electrons[20] begins to affect the ion drift velocity. As is well known from the physics of gas discharge at high avalanche densities ($\geqslant 10^{12}$ cm^{-3}), ambipolar diffusion can lead not only to complete vanishing of the ion drift velocity, but also to a change of the direction of the ion motion.[21]

Since the ions and electrons in the avalanche overlap and drift with different velocities in opposite directions, the drift in the avalanche unavoidably leads to charge separation and to the appearance of an electric field which tends to oppose this separation. The higher the avalanche density, the smaller the scales of the charge distribution in space and time, and

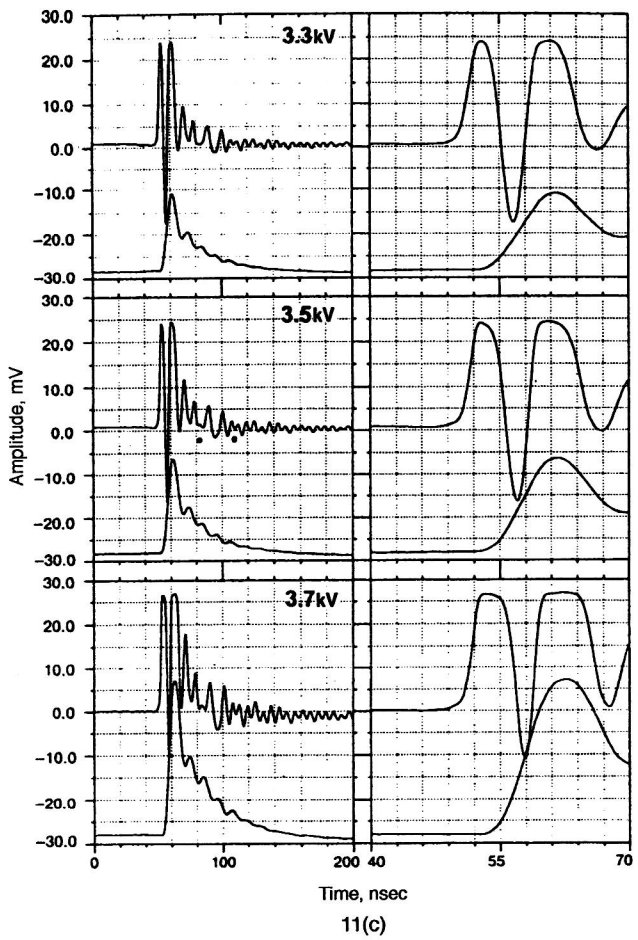

11(c)

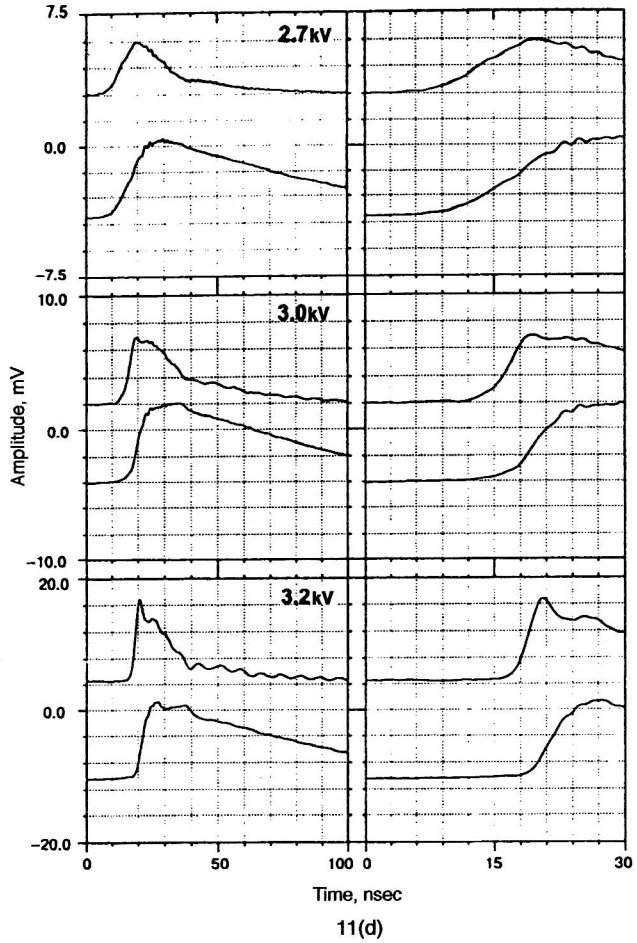

11(d)

FIG. 11 (*Continued.*)

the stronger the manifestation of the automatic mechanism for balancing charges of opposite signs. The motion of the particles in the avalanche is such that the ions cannot be separated from the electrons.[17] If the potential difference over the separation length becomes comparable in magnitude to the potential difference created over this length by an external source, the ion and electron velocities will be close to zero. As the avalanche develops, the process will grow and propagate in the direction toward the anode, owing to the growth of the charge density and the more intense electron bremsstrahlung. The tendency to establish quasineutrality causes an ever larger part of the slow electrons to be decelerated, both inside the positively charged cloud and at the avalanche front as the avalanche develops. This process naturally tends to weaken the effect of the external field inside the avalanche, owing to Coulomb screening (2) (Ref. 42). Meanwhile, the conditions change dramatically for part of the front electrons, owing to the increased field between the electrons and the anode: the electrons pass into the regime of continuous acceleration (see Fig. 9) and intensively ionize the gas molecules, because the electrons stopped by the ion cloud, which are located in front of the cloud, will enclose the ions formed by the fast electrons.[21]

The picture described above is a part of the dynamics of avalanche development, and it is important from the viewpoint of the process of signal formation at the chamber electrodes. Actually, why does the cathode signal appear in the chamber simultaneously with the other signals for low gain, while it begins to be delayed at higher gas gains? If all the analyzed signals correspond to the same current through the chamber and the external circuit, then, according to the Ramo–Shockley theorem,[5] these signals must always appear simultaneously. On the other hand, as mentioned above, the movement of the charges to the anode is screened from the cathode by the practically stationary ion layer. If this is true, then no current at all can flow in the circuit as long as screening is present. Nevertheless, signals are formed at the anodes. The reason is the following. In wire chambers the density of avalanche particles in the direction toward the anode is strongly nonuniform, and the high avalanche density creates strong screening of the charges from the external electric field. This necessarily induces a diffusion current, which tends to eliminate the resulting density gradient. As a rule, the total current should consist of the drift and diffusion parts. Here the densities of the electron and ion fluxes are given by[21]

$$\Gamma_{\pm} = \pm n_{\pm}\mu_{\pm}E - D_{\pm}\nabla n, \tag{8}$$

where μ and D are the mobility and diffusion coefficients for electrons and ions, E is the electric field, equal to the sum of

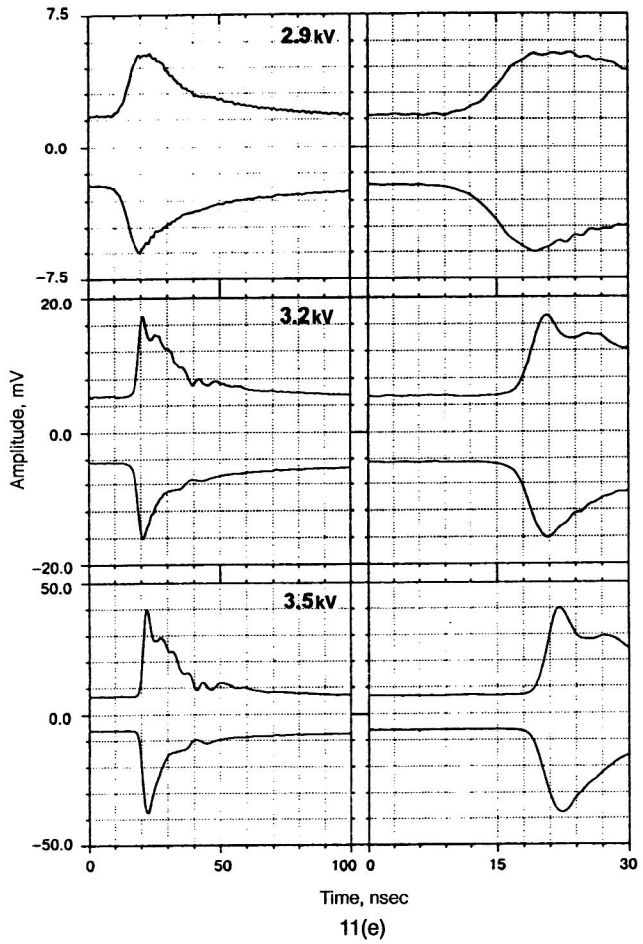

FIG. 11 (*Continued.*)

the external field and the polarization field induced by the charge separation and the density gradient, and n is the particle density per unit volume.

The current density j in this situation is found from (8) (Ref. 21):

$$j=e(\Gamma_- -\Gamma_+)=(D_- -D_+)e\nabla n+(\mu_- +\mu_+)Een, \quad (9)$$

and the electric field, equal to the sum of the external field responsible for the current through the chamber and the polarization field induced by the presence of gradients in the avalanche, is given by

$$E=\frac{j}{e(\mu_- +\mu_+)n}-\frac{D_- -D_+}{\mu_- +\mu_+}\cdot\frac{\nabla n}{n}. \quad (10)$$

Since $D_- \gg D_+$, for strong screening of the external field in the avalanche the current density will mainly be determined, according to (9), by the diffusion part $j\approx eD_-\nabla n$, i.e., the principal current source will be free electron diffusion.[21] Therefore, returning to our problem, we see that if there is no current in the circuit, the external source will not complete its separation of the bound charges, and the electrons inside the avalanche will not acquire energy from the field and cannot pull the ions behind them. Put differently, a dynamical system undergoing rapid development over several nanoseconds begins to be conservative. The process continues as long as there is no diffusion current. The charge acquired by the anode wire 2 (Fig. 1) as the drifting front electrons and the diffusing electrons reach it induces, by electrostatic induction, a redistribution of the charges of opposite sign over all the adjacent wires, the electric field of which decreases the potential of wire 2. The potentials of wires 1, 3, and the others are raised. The resulting electric field varies in time according to the variation of the charge reaching the anode wire 2 from the avalanche. The anode wires are coupled together capacitatively and, as a rule, are connected via load impedances to a common conductor running to the positive side of the high-voltage source. Since there is no current through the source and the chamber, owing to the varying electric field the diffusion electron current will enclose the adjacent anode wires via the inter-anode capacitances and load impedances. Here the current passing through the impedance of wire 2 is equal to the sum of the currents passing through the other impedances.

Practically when the electron current begins to flow, enhancement of the anode screening by the space charge of the ions begins, which tends to lower the external field near the anode and raise it in going toward the cathode. Under the action of the density gradient and the enhanced electric field, the ions of the cloud and the electrons bound to them begin to be shifted from the region with higher density and weaker field to the region with lower density and stronger field, i.e., ambipolar diffusion and ambipolar drift of the charges along the nonuniform electric field begin. The ambipolar charge flux is characterized by the ratio[21]

$$\frac{D_E}{D_a}=\frac{E^2}{4\pi nkT}=\frac{\{E[\mathrm{V/cm}]\}^2}{1.8\times 10^{-6}nT[\mathrm{eV}]}, \quad (11)$$

where D_E is the effective diffusion coefficient for ambipolar drift, and D_a is the ambipolar diffusion coefficient.

We see from (11) that in wire chambers ambipolar drift begins to dominate over ambipolar diffusion if the field of the space charge is $E>10^2$ V/cm, and the particle concentration in the avalanche is $n=10^{10}$ cm^{-3}. These values are realized in a wire chamber already for a gas gain of 10^5.

The velocity of the ambipolar flux will be[43]

$$v=\mu_+E-\frac{D_+}{n_+}\frac{dn_+}{dx}, \quad (12)$$

where E is the electric field along the ion motion, equal to the sum of the external field and the space-charge field.

The transfer of space charge in the direction of the avalanche tail sets the electrons held by the screening ion layer into motion, which, in turn, allows this layer to begin to move to the cathode and, generating its polarization, to induce a current in the entire circuit. The electrons freed from the ion layer will be partially stopped in the dense ion cloud.

In conclusion, let us estimate the scale of the charge separation in the screening layer. For a chamber voltage of 2.5 kV and a gas filling of 80% CF_4+20% C_4H_{10}, the delay of the cathode signal is $t\approx 6$ nsec (Fig. 11a). The time jitter of the anode signals in this case is $\Delta t=9.2$ nsec (Fig. 8a). Since the jitter is completely determined by the time fluctua-

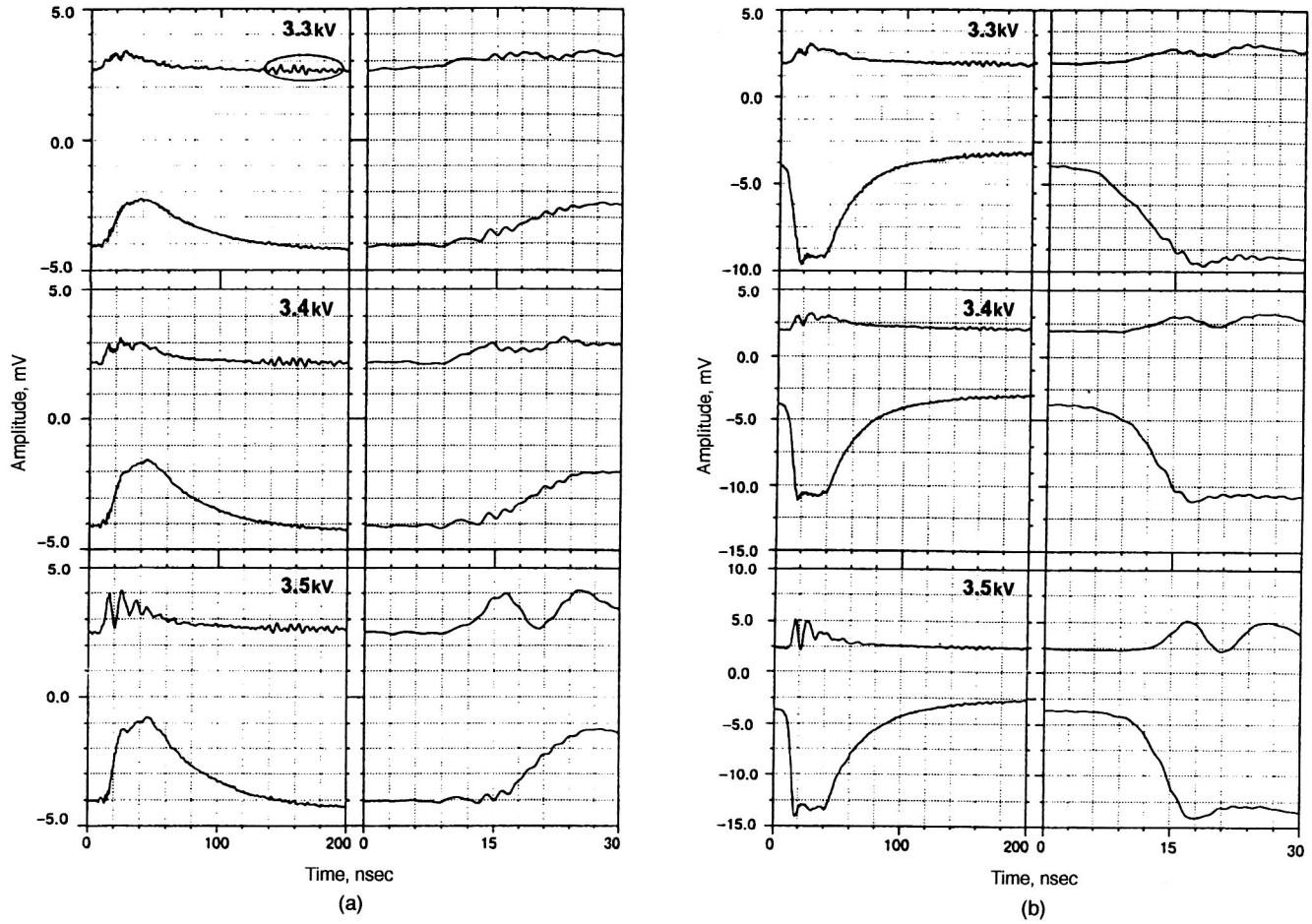

FIG. 12. Oscillograms of signals from the control wires (upper figures) and from the cathode (a) or anode (b) for chamber filled with the gas mixture 70% Ar+30% C_4H_{10}. The chamber voltage is given on the oscillograms. The cathode signals (lower oscillograms) are decreased by 20 dB (a), and the anode signals by 12 dB (b).

tions of the drift of the first electrons produced near the anode plane over a length equal to half the anode spacing S (Ref. 32), the electron drift velocity will be

$$\frac{S}{2\Delta t}=\frac{0.1}{9.2\times 10^{-9}}=1.1\times 10^{7}\ \text{cm/sec}. \tag{13}$$

For this velocity, the electron layer during the first nanosecond of the cathode-signal delay is shifted relative to the ion layer by a distance $10^{-9}\times 1.1\times 10^{7}=1.1\times 10^{-2}$ cm. In fact, the real separation length must be considerably smaller, because while moving the electrons feel the effect of retarding Coulomb forces. Their drift velocity will therefore fall and completely vanish when, as noted above, the potential difference over the separation length becomes zero. From this instant the state and configuration of the electron layer will be determined by the state of the ion layer.

8.2. The avalanche development time

The signals produced at the control wires give information about this very important characteristic of an avalanche. According to the oscillograms shown in Figs. 11–14, the avalanche development time τ_a is equal to the time for the first peak (upper oscillogram) to rise to its maximum amplitude. The structure in the oscillograms beyond the first peak corresponds to other processes arising in the avalanche after it is complete. These processes will be studied in Sec. 8.3.

We see clearly in the oscillograms that the avalanche development time depends both on the value of the gas gain in the chamber, and on the gas composition. The very low rate of avalanche development in the initial stage associated with the diffusion current is common to all gas mixtures and is practically independent of the gas gain (see Sec. 8.1). The time for this stage is almost half the total avalanche development time and ranges from 2.5 nsec for the mixture 80% CF_4+20% C_4H_{10} at τ_a=5 nsec to 5 nsec for the mixture 95% CF_4+5% C_4H_{10} at τ_a=12 nsec. On the other hand, as the gain increases, in all gas mixtures τ_a tends to a limit of 4.5 nsec. However, this limit is reached in each mixture for different values of the gas gain (Fig. 15).

An interesting by-product of these results is the fact that the limiting value of τ_a in each gas mixture is reached at a gas gain corresponding to the maximum delay of the cathode signals.

If the avalanche reaches its minimum development time, this implies that the speed at which the bulk of the electrons move during deceleration by the volume charge reached its minimum value, after which the electrons are effectively bound by ions. It is from this moment on that further gain in

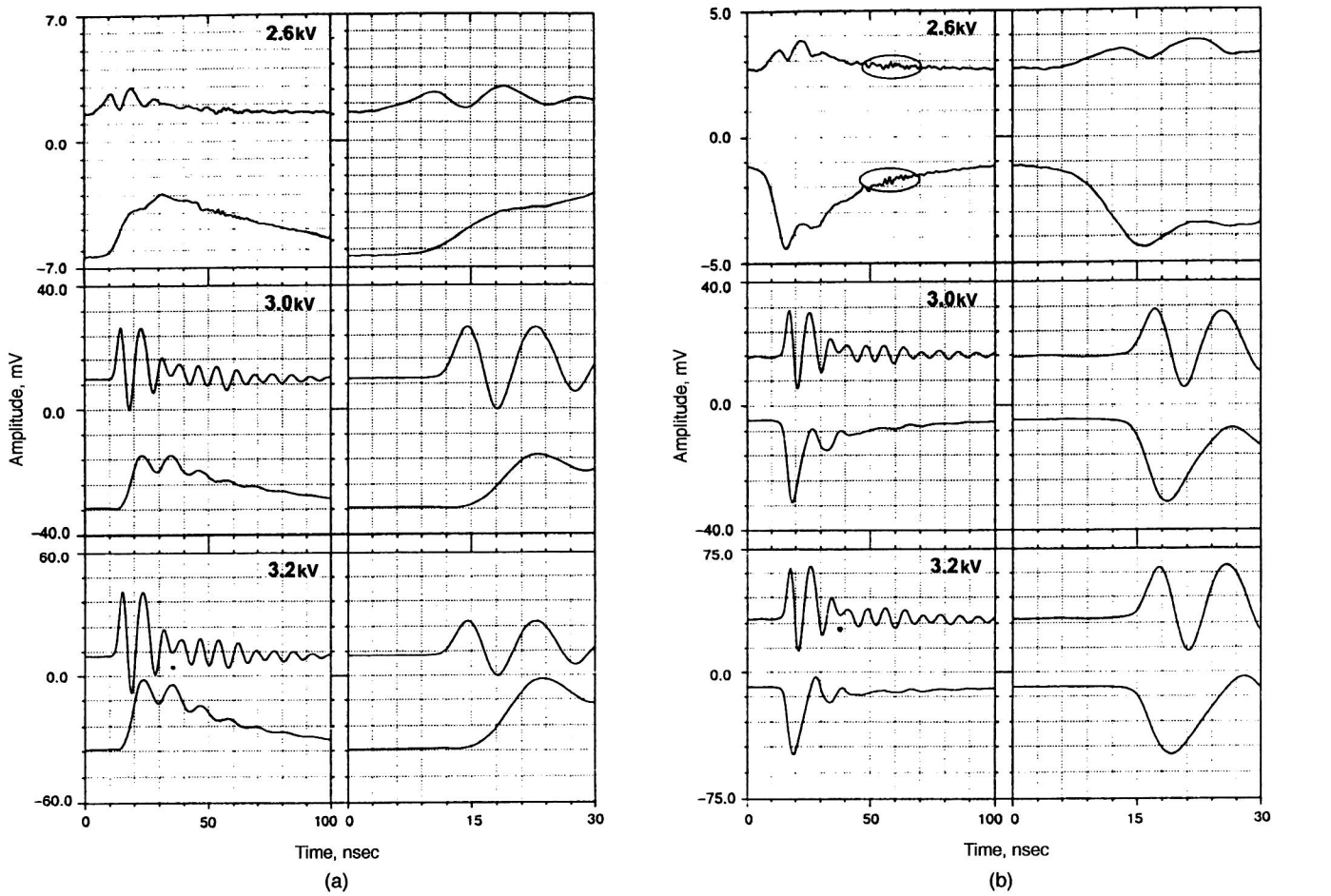

FIG. 13. Oscillograms of signals from the control wires (upper figures) and from the cathode (a) or anode (b) for chamber filled with the gas mixture 85% CF_4+13% C_4H_{10}+2% $CO(CH_3)_2$. The chamber voltage is given on the oscillograms. The cathode signals (lower oscillograms) are decreased by 10 dB (a), and the anode signals by 12 dB (b).

the avalanche occurs mainly owing to the front electrons, for which, as noted in Sec. 8.1, the conditions are favorable.

We see from Fig. 15 that the required avalanche density at which the charge deceleration and binding are complete is reached at different gas gains in different gas mixtures: the heavier the gas, the smaller the gain and the earlier the time at which that density is reached. The further change of the particle density in the avalanche will be determined only by the remaining distance to the anode which must be traveled by the front electrons. Information about the avalanche development time before saturation is reached is very useful (Fig. 15), because this time closely reflects the behavior of the electron drift velocity in the avalanche-production region for increasing influence of the space charge on the electrons.

The apparent decrease of the time for electron collection at the anode of the chamber (Fig. 8b) is actually due to the strong decrease of the signal front with increasing voltage. We see clearly from the oscillograms that as the voltage increases to 3.5 kV the duration of the anode-signal front in Figs. 13b and 14b is decreased by more than a factor of two, and is equal to 6 nsec and 11 nsec, respectively. For this reason, all the oscillograms are shifted to the right with increasing voltage.

8.3. Electrostatic oscillations of the ions and ion sound

In Sec. 8.1 it was noted that the motion of the electrons supported by the screening ion layer is associated with transfer of the ion cloud in the direction of the cathode. This process occurs over a time determined by the cathode-signal delay time. If the delay time t_d is smaller than the avalanche development time τ_a, the avalanche development continues. The equality $t_d = \tau_a$ implies that the process of ionization by electrons moving at the front of the avalanche is completed in a time t_d. Here, as long as the avalanche is developing, a part of the avalanche electrons goes to the anode, owing to the diffusion current, and a neutralized ion cloud remains in the avalanche-production region.

The transfer of the ion cloud to the cathode owing to ambipolar diffusion and ambipolar drift tends to increase the external field between the cloud and the anode. The slow electrons located in the cloud begin to undergo ambipolar drift to the anode owing to the increase of the field. This drift unavoidably leads to the appearance of a restoring force proportional to the displacement of the electrons trying to break through to the anode. However, the electrons, which acquire

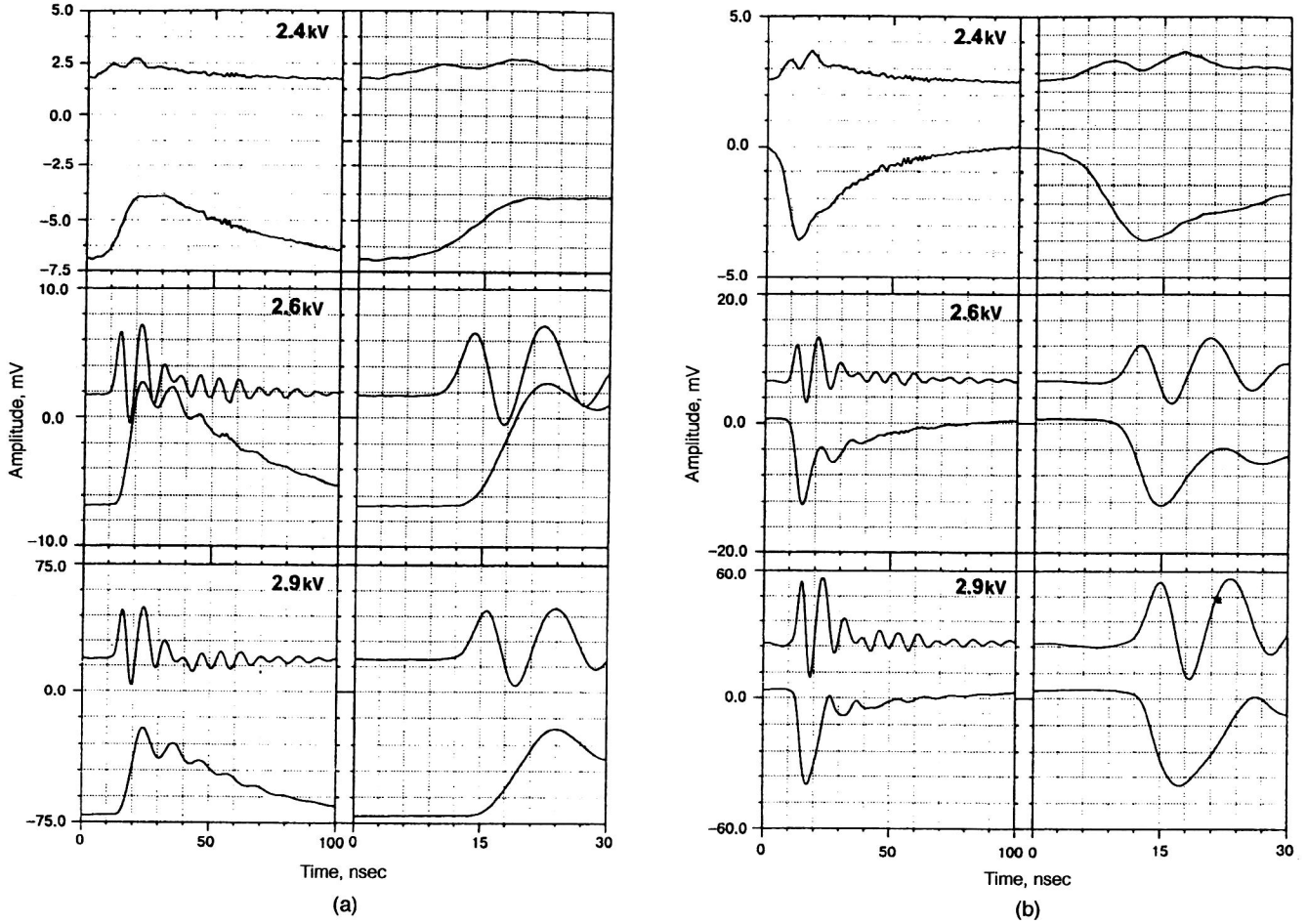

FIG. 14. Oscillograms of signals from the control wires (upper figures) and from the cathode (a) or anode (b) for chamber filled with the gas mixture 90% CF_4+10% C_4H_{10}+2.5×10^{-4} Hg. The chamber voltage is given on the oscillograms. The cathode signals (lower oscillograms) are decreased by 10 dB (a), and the anode signals by 12 dB (b).

more and more energy from the increasing external field along their path, will be forced to expend a part of this energy on the ions in order to pull them along and thereby group them into a dense bunch. After these electrons go to the anode, the repulsive force between the anode and the dense ion cloud sharply increases. This force will act in opposite directions on the electrons and on the ions of the cloud. These processes are also directly illustrated by the upper oscillograms, obtained from the control wires.

The sharp decrease of the amplitude of the first peak (i.e., the change of the current direction) after the maximum value is reached indicates that the neutralized ion cloud moves behind the drifting electrons in the direction toward the anode under the action of the thermal electron pressure and the separation field. The high degree of neutralization of the ion cloud is also indicated by the weak change of the signal amplitude at the anode of the chamber. We see from the oscillograms that during the periodically varying signals at the control wires, the amplitude of the anode signals is increased by only 10–20%, while at the cathode a strong dependence of the signal amplitude on the periodic variation of the induction charge is observed. This is most likely related to the neutralization of the cloud mainly along the avalanche axis. In all the other directions the charge induction associated mainly with the ion motion gives a significant contribution.

Under the action of the repulsive force, the ions begin to move toward the cathode, while the electrons in the cloud dragged by the external field drift to the anode. The charge separation leads to a restoring force. However, the electrons,

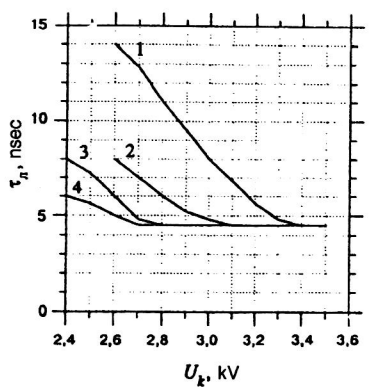

FIG. 15. Dependence of the avalanche development time on the chamber voltage for various gas mixtures filling the chamber: (1) 95% CF_4+5% C_4H_{10}; (2) 85% CF_4+13% C_4H_{10}+2% $CO(CH_3)_2$; (3) 90% CF_4+10% C_4H_{10}+2.5×10^{-4} Hg; (4) 80% CF_4+20% C_4H_{10}.

which are highly mobile and supported by the anode, adiabatically adapt to the ion displacements, affecting the ion motion. As a result, the combined action of the pressure forces of both the electrons in the ion cloud and the electric field of the charge separation leads to wave motion of the ions.[16,17,20]

Before discussing these results further, it will be useful to review briefly the main features of electrostatic oscillations in a plasma.[16,17,41]

It is well known from plasma physics that the displacement of unequally charged particles in opposite directions, i.e., their separation, leads to the appearance of a local electric field, which produces charge oscillations. The combined displacement of the charges of both signs in the same direction leads to a localized region of increased pressure, which generates elastic oscillations (like sound waves).

When discussing plasma oscillations in plasma physics, one usually has in mind high-frequency electron oscillations in which the ion motion is neglected. The expression for the electron plasma frequency has the form

$$\omega_0=\sqrt{\frac{4\pi ne^2}{m}};\quad f=\frac{\omega_0}{2\pi}=8960\sqrt{n}, \tag{14}$$

where n is the electron density. For example, for $n=2\times10^{13}$ cm^{-3}, the frequency of electrostatic plasma oscillations of the electron branch will be $f_0=4\times10^{10}$ sec$^{-1}=40$ GHz. The dispersion equation for the low-frequency branch of plasma oscillations arising as a result of the ion motion has the form

$$\omega^2=\frac{k^2\omega_0^2\dfrac{\gamma_eT_e+\gamma_iT_i}{M_i}+k^4\gamma_e\gamma_i\dfrac{T_eT_i}{m_eM_i}}{\omega_0+k^2\left(\gamma_e\dfrac{T_e}{m_e}+\gamma_i\dfrac{T_i}{M_i}\right)}, \tag{15}$$

where k is the wave number, T_e and T_i are the electron and ion temperatures in energy units, and γ_e and γ_i are the adiabatic exponents. Equation (15) is written for singly-charged ions.

In the limiting cases for the wave number, when $k\to0$ or ∞, the low-frequency branch (15) gives ion sound with slightly different dispersion relations:

(1) For long wavelengths ($k\to0$):

$$\omega^2\approx k^2\frac{\gamma_eT_e+\gamma_iT_i}{M_i}. \tag{16}$$

(2) For short wavelengths ($k\to\infty$):

$$\omega^2\approx k^2\gamma_i\frac{T_i}{M_i}. \tag{17}$$

Equations (16) and (17) differ in that in the case of long wavelengths the electrons also participate in the propagation of ion sound, but they move as though each of them had mass M_i.

(3) Let $T_i\to0$, and the wave number and temperature of the electrons be constant (it should be noted that the conditions of this case are well satisfied in an electron avalanche produced in a wire chamber). In this limiting case Eq. (15) takes the following form for short wavelengths:

$$\omega^2\approx\frac{m_e}{M_i}\omega_0^2. \tag{18}$$

Therefore, instead of ion sound we have purely electrostatic oscillations of the ions:

$$\omega=\sqrt{\frac{4\pi ne^2}{M_i}}. \tag{19}$$

Equation (19) also determines the ion plasma frequency, which arises as a result of the displacement of the ions in the self-consistent electric field of the electrons and is determined by the long-range Coulomb interaction of the ions.

Therefore, for sufficiently cold ions, but hot electrons, in a wide range of wavelengths the ion branch is purely electrostatic in nature. In this range the ions oscillate with constant electrostatic frequency. However, in going away from this branch either toward long or toward short wavelengths, the electrostatic oscillations of the ions become ion sound.[17,41]

The frequency of the electrostatic oscillations of cold ions is such that the ions appear to be shifted, while the electrons are stationary. In fact, the electrons are always much more mobile than the ions, but if the electrons are hot, the thermal motion smears the electron concentration uniformly over space. In this case the ion oscillations occur on a uniform electron background.[17,41]

In Fig. 16 we give the oscillograms from the control wires in the range up to 30 nsec, measured for chamber voltages of 2.6 kV and 2.9 kV, respectively, but for different gas mixtures. Figure 17 demonstrates the behavior of the signals at the control wires as a function of the chamber voltage for the gas mixtures 90% CF_4+10% C_4H_{10}+2.5×10^{-4} Hg and 85% CF_4+13 C_4H_{10}+2% $CO(CH_3)_2$, respectively. For convenience in comparing the frequency characteristics and their dependence on the gas content and the chamber voltage, the signal amplitudes were varied proportionally in such a way that the amplitudes of the first peak coincide for different oscillograms. Therefore, the amplitude characteristics of the oscillograms in Figs. 16 and 17 display only the time and frequency characteristics and the values of the oscillation periods, and also the duration of the avalanche development. Comparing the oscillograms, we see that the frequency of the ion oscillations depends on the gas content and varies from 116 MHz to 133 MHz (Fig. 16). As the chamber voltage changes for fixed gas filling, a change of the oscillation frequency from 119 MHz to 125 MHz (Fig. 17a) and from 106 MHz to 120 MHz (Fig. 17b) is also observed. This behavior of the oscillation frequency indicates that the average electron energy is different in different gas mixtures for a given chamber voltage. A change of the electric field in the chamber causes the average electron energy for fixed gas mixture to change.

These dependences represent information useful for the physics of gas discharge in molecular gases, since they can be used to obtain information about the average electron thermal velocity, which is associated with the drift velocity and with the electron energy losses in a given gas [see Eq. (6)].

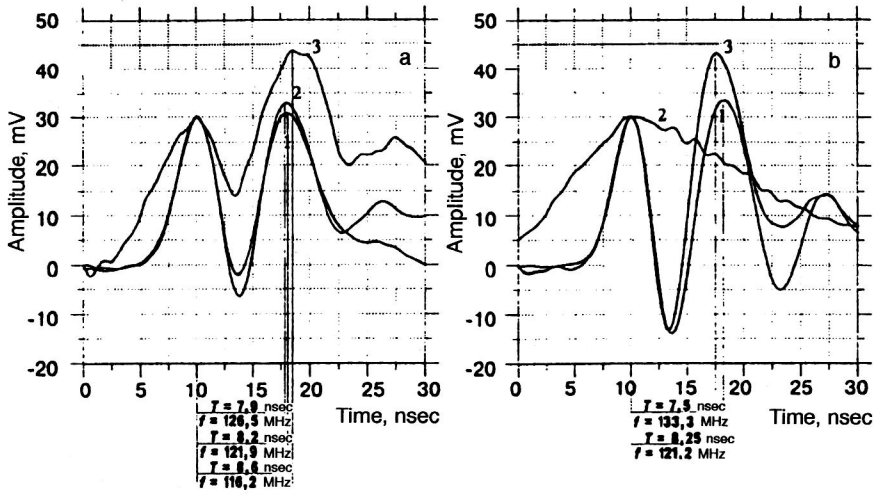

FIG. 16. Frequency of ion plasma oscillations in various gas mixtures for chamber voltage (a) 2.6 kV: (1) 95% CF_4+5% $CH_3CH_2(OH)CH_3$; (2) 96% CF_4+4% $CO(CH_3)_2$; (3) 85% CF_4+13% C_4H_{10}+2% $CO(CH_3)_2$; (b) 2.9 kV: (1) 90% CF_4 +10% C_4H_{10}+2.5×10^{-4} Hg; (2) 95% CF_4 +5% C_4H_{10}; (3) 80% CF_4+20% C_4H_{10}.

Knowing the frequency of the ion oscillations, (19) can be used to determine the ion density in the ion cloud. For example, for the gas mixture 80% CF_4+20% C_4H_{10} (Fig. 16b), the linear frequency of the ion oscillations is $f=133$ MHz. The angular frequency will be $\omega=2\pi f=837.5$ MHz. From (19) for the ion density we have $n_i=2.1\times10^{13}$ cm^{-3}.

Knowing the avalanche density, we can estimate its spatial extent. Direct measurements of the amplitude of the anode signal for a resistance of 50 Ω give average values of 50 mV for a chamber voltage of 3.2 kV (Fig. 6). For the width of the signal at half-max equal to 5×10^{-9} nsec, the number of particles in the avalanche is $n=It/e=3.1\times10^7$. The volume of the avalanche for a given number of charge carriers will be $n/(n_i+n_e)=7.4\times10^{-6}$ cm^3. The length of the avalanche-production region (Fig. 3), given by the condition that the threshold value of the electric field is 20 kV/cm, is 0.03 cm. Therefore, $0.03\cdot(\Delta y\cdot\Delta z)=1.5\times10^{-6}$ cm^3, or $\Delta y\cdot\Delta z=0.5\times10^{-4}$ cm^2. Assuming that the avalanche is symmetric about the x axis, we have $\Delta y=\Delta z=0.7\times10^{-2}$ cm^2. Since during its development the avalanche gradually expands and becomes cigar-shaped, knowing the avalanche volume we can easily transform a parallelepiped into the approximate shape of the avalanche.

The values obtained above allow such important parameters of a high-current avalanche as the Debye radius and the electric field in the charge-separation region to be estimated.

If the linear dimensions of the separation region have scale x and the concentration of charged particles in the avalanche is n, then[40]

$$\operatorname{div} E\approx\frac{E}{x}=4\pi ne,\quad E=4\pi nex. \tag{20}$$

As the electric field of the charge separation increases, the diffusion becomes ambipolar if a significant drop of the charge density occurs over distances larger than the Debye screening radius.[39] This condition is expressed as[21]

$$\frac{\delta n}{n}\approx\frac{kT_e}{4\pi ne^2}\cdot\frac{1}{R}=\left(\frac{r_D}{R}\right)^2,\quad r_D=\left(\frac{kT_e}{4\pi ne^2}\right)^{1/2}=6.9\left(\frac{T_e}{n}\right)^{1/2}, \tag{21}$$

where R is the characteristic dimension of the region where the charge density drops strongly (i.e., the avalanche length), r_D is the Debye screening radius, T_e is the electron temperature (the average thermal energy), and n is the concentration of charge carriers in the avalanche.

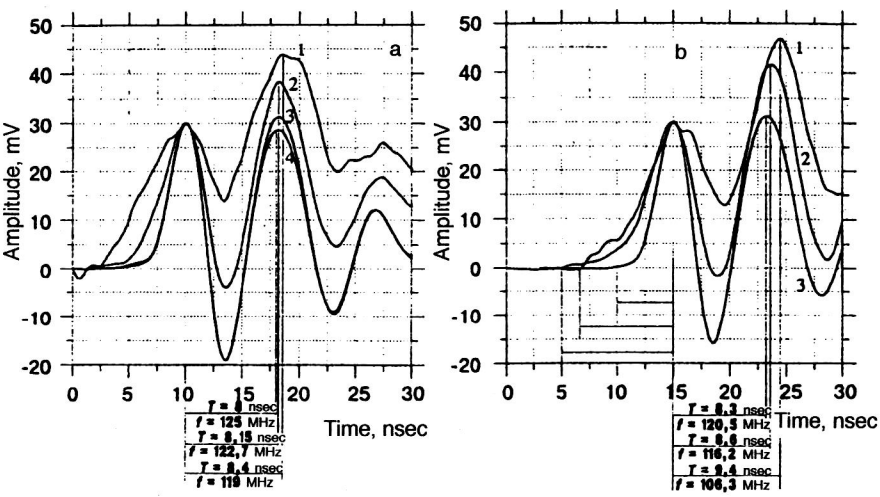

FIG. 17. Frequency of ion plasma oscillations for chamber filled with the gas mixture (a) 90% CF_4+10% C_4H_{10}+2.5×10^{-4} Hg for various chamber voltages: (1) 2.6 kV; (2) 2.8 kV; (3) 3.0 kV; (4) 3.2 kV; (b) 85% CF_4+13% C_4H_{10}+2% $CO(CH_3)_2$: (1) 2.45 kV; (2) 2.5 kV; (3) 2.9 kV.

If the current in the external circuit is zero or small compared with the electron diffusion current [separation field in (10) comparable to the external field], the avalanche will be quasineutral in the case $R \gg r_D$, and so $\delta n/n \ll 1$. Therefore, the criterion for quasineutrality will be[21]

$$\left(\frac{r_D}{R}\right)^2 \ll 1, \tag{22}$$

which implies that the charge-separation field which appears prevents the violation of quasineutrality at distances larger than the Debye screening radius.

Let us estimate the Debye radius for our case. According to Ref. 44, the average thermal energy of the electrons in the gas mixture 80% CF_4+20% C_4H_{10}, corresponding to the minimum in the electron scattering cross section in CF_4, is 0.2 eV. According to (21), the Debye radius will be $r_D = 1.8 \times 10^{-4}$ cm. For charge separation by a distance equal to r_D, a field $E = 4\pi n e r_D \approx 7000$ V/cm arises. If the separation scale grows to $10r_D = 18 \times 10^{-4}$ cm owing to the effect of the density gradients, the external field, and the high electron mobility, the separation field will be 7×10^4 V/cm and will make up 35% of the field in the chamber at a distance of 18×10^{-4} cm from the anode. According to (22), for such a charge separation the quasineutrality of the avalanche is preserved:

$$\left(\frac{10r_D}{R}\right)^2 = \left(\frac{18 \times 10^{-4}}{3 \times 10^{-2}}\right)^2 = 3.6 \times 10^{-3} \ll 1. \tag{23}$$

The average thermal energies of the electrons differ slightly from each other in the gas mixtures used. Therefore, as the avalanche density decreases the screening length grows, approaching the wavelength of the ion oscillations. It follows from the expression for the damping coefficient for the ion oscillations,

$$\delta \approx \frac{\sqrt{\pi}\omega}{2\sqrt{2}} \left(\frac{\lambda}{2\pi r_D}\right)^3 \cdot e^{-\lambda^2/8\pi^2 r_D^2}, \tag{24}$$

that if r_D approaches or is equal to the wavelength $\lambda \approx (\pi T_e/ne^2)^{1/2}$, the damping will occur over a time of the order of the oscillation period.[17] The ion oscillations illustrated in the oscillograms are in good agreement with this conclusion. We see that the oscillations occurring in all the gas mixtures except 80% CF_4+20% C_4H_{10} last no more than two periods. In this mixture the oscillations last for six periods.

The behavior of the oscillations about the equilibrium position is also interesting. Here there is also a dependence on the avalanche density. When the chamber is filled with the gas mixture 85% CF_4+13% C_4H_{10}+2% $CO(CH_3)_2$, the positive and negative oscillation phases are practically symmetric (Fig. 13). Replacement of saturated acetone vapor by mercury vapor (Fig. 14) causes the positive phase to grow and the negative phase to fall. For the gas mixture in Figs. 11a–11c we see practically complete asymmetry on the side of the positive phase. The asymmetry is most likely related to the direction of the electron pressure in the avalanche and is a manifestation of the decelerating force (Coulomb friction), induced by the growing electron interactions at the instant when the wave is compressed, and also to the action of the wave field on the charged particles of the ion cloud.

The particles in the avalanche have velocities both smaller and larger than the phase velocity of the wave. The action of the field of a leading wave on particles with smaller velocity is to transfer a momentum to them, so that the wave pulls the particles along. Particles moving faster than the wave lose momentum to the wave. As a rule, the number of particles pulled by the wave is larger than the number of particles transferring momentum to the wave.[20] The result is rapid damping of the plasma oscillations of the ions and their transformation into ion sound. It follows from plasma physics that the propagation of ion sound without damping is possible only when the electron temperature is much higher than the ion temperature.[17]

The instant at which the ion oscillations are transformed into ion sound is indicated by a dark point on some of the oscillographs. For gas mixtures containing acetone and mercury, the duration of the ion-sound oscillations in a quasineutral cloud is about 60–65 nsec. For the mixture 80% CF_4+20% C_4H_{10} the ion-sound oscillations (Fig. 11b) last more than 100 nsec. The frequency of the oscillations in this case is about 25% higher than in other gases. We see from the oscillograms (Figs. 11e and 12a) that ion and sound oscillations are practically absent in the gas mixtures 70% Ar+30% C_4H_{10} and 95% CF_4+5% C_4H_{10}.

The dependence of the duration of the anode and cathode signals on the rate of buildup of the ion oscillations should be noted. We see from Figs. 11–14 that as the amplitude of the oscillations grows, the duration of the anode and cathode signals decreases, and at the same time their shapes change. These changes are clearly expressed in gas mixtures in which plasma oscillations of the ions appear and are clearly related to them. During the buildup of the oscillations the duration of the anode signal becomes roughly equal to the period of the oscillations in the region with maximum amplitude. Owing to the smallness of the subsequent oscillations, their effect on the signal shape is unimportant. The effect of ion oscillations on the cathode signals is integrated, owing to the large cathode capacitance relative to ground.

Measurements using the γ source ^{55}Fe were made to compare the effect of the primary ionization on the characteristics of plasma production. These measurements showed that plasma oscillations of the ions in the avalanche begin about 300 V earlier in this case. No other features characteristic of this type of source compared with the radioactive β source ^{90}Sr were found.

In conclusion, let us show that the ion oscillations in a quasineutral cloud are small. It will be shown in Sec. 8.4 that in the oscillation process the average ion energy reaches 0.2 eV, which corresponds to an ion velocity of 8.5×10^4 cm/sec. At this velocity the displacement of the oscillating ions from equilibrium at oscillation frequency 133.5 MHz over half a period will be $vT/2 = 3.2$ μm. Owing to the asymmetry of the oscillations (Figs. 11b and 11c), the ions will oscillate mainly between the anode and the equilibrium position.

8.4. Streamer formation and the mechanism for its growth toward the cathode

In Sec. 6.1 it was shown that as the gas gain increases there is a tendency for the anode and cathode signals to increase by a jump. According to Ref. 35, the jump in the signal amplitudes is associated with the appearance of a streamer. However, the mechanism for streamer formation was not clearly described either in Ref. 35, or in the many other studies (Refs. 7, 18, 36, and 45). Basically, there is no clear explanation of the conditions for the transformation of an electron avalanche into a streamer or for the appearance of secondary electrons ahead of the streamer propagation front.

The dynamics of these complicated processes can be understood only by carefully studying all the phenomena which favor this transformation. It follows from the preceding section that the spatial structure of an avalanche at gas gain 10^6 cannot be viewed as a set of two oppositely charged clouds, because the action of the long-range Coulomb forces in the end causes the charges to mix, which, in turn, favors transformation of the avalanche into a quasineutral plasma. In this new state of a quasineutral plasma there will be more intense heat-exchange processes between the avalanche particles, the accelerations in the external field will be equalized, and the interdependence of the particle motions will become more pronounced.

However, transformation of an avalanche into a quasineutral plasma is still not sufficient for initiating streamer formation. It is also necessary that the density of charge carriers in the plasma cloud exceed some threshold value. If the latter condition is not satisfied, accelerated electrons will practically not be produced in the avalanche. Their absence is reflected in the low degree of neutralization of the ion cloud, because slow electrons will not be screened from the anode. In the end, the plasma oscillations of the ions will be rapidly damped out, and the plasma will become unstable even for small spatial redistributions of the charged particles. The oscillograms shown in Figs. 13a and 14a provide an example of this. We see that even the insignificant increase of the density of the gas mixture when acetone is replaced by mercury (which is heavier and more active in avalanche development) leads to an obvious change of the characteristics of the plasma cloud, expressed as growth of the positive oscillation phase. The required conditions are met most completely by the gas mixture 80% CF_4+20% C_4H_{10}. Large values of the gas gain are attained for it. A high avalanche density, manifested in the delay of the electrons by the ion field (the regime of ambipolar diffusion), is realized practically at the start of the proportional regime. As the gain increases, the duration of the plasma oscillations of the ions grows and, beginning at a gain of about 4×10^7 (U_{ch} = 3.5 kV), the avalanche development enters a new stage. This is expressed as the clear separation of the avalanche electrons into two groups (Fig. 9), the beginning of an amplitude jump (Fig. 7b), and the start of the second stage of plasma oscillations of the ions. The time interval of the second series of oscillations is indicated by the two dark points in Fig. 11c.

The existence of a delay of about 27 nsec between the time at which the first avalanche is completed and the start of the second (Fig. 11c) is most striking. The magnitude of this delay depends strongly on the degree of localization of the avalanche. If a gap collimator with a gap of 0.15 mm is placed directly opposite the anode wire 2 (Fig. 1), the maximum avalanche density and a delay of about 10 nsec are ensured. Moving the collimator to the left or to the right of the wire leads to smearing of the avalanche, because clusters from ionization drifting along different lines of force form a less dense avalanche than in the former case. According to these measurements, the range of delays for this gas is 10–30 nsec. Nearly the same times between the instant at which the avalanche is completed and the instant at which the streamer is formed were obtained in Refs. 46 and 47.

It should be noted that the fraction of avalanches containing fast electrons depends strongly on the degree of localization of the avalanche. For high localization (source opposite wire 2), the number of avalanches with fast electrons is about 45%. As the avalanche density decreases (the source is moved 0.8 mm to the left of the wire), the fraction of avalanches with fast electrons falls to 20%.

The presence of a delay between avalanches apparently plays a very important role in streamer formation. This time interval may be necessary owing to the nonequilibrium state of the plasma cloud, in which spontaneous transitions to the equilibrium state must unavoidably arise. It follows from the dynamics of avalanche formation in a nonuniform field that the density, pressure, and temperature gradients are most strongly expressed in this medium. As shown above, the presence of gradients inside the avalanche leads to macroscopic motions which cause the ions to oscillate. When these oscillations begin, the pressure from the wave propagating along the plasma cloud is added to the thermal pressure of the electrons ($p=n_-kT_-$) acting on the ions. The oscillograms shown in Figs. 11a–11c clearly reflect the dynamics of the processes occurring in the avalanche as a function of the high chamber voltage. We see that for chamber voltages of up to 3.0 keV the amplitude of ion-sound waves in the plasma cloud grows linearly. The oscillations are supported by the inflow of energy from the external field. The energy carriers are electrons. The increase of energy inflow to the wave due to electron multiplication causes the oscillation amplitude to grow.

It was noted in Sec. 8.1 that the elimination of the screening layer in the direction of the cathode by the slow diffusion current induces a current through the chamber. This current causes the electron velocity distribution to shift to higher drift velocities. The decrement of the damping of ion–sound oscillations in a plasma with directional electron flux is[53]

$$\gamma_s^e(\mathbf{k})\left(1-\frac{\mathbf{k}\mathbf{v}_d}{kv_s}\right)=\gamma_{s0}(\mathbf{k}), \tag{25}$$

where $\gamma_s^e(\mathbf{k})$ is the electron-induced decrement of linear Landau damping for ion-sound waves, $\mathbf{v}_d$ is the average electron drift velocity, and v_s is the ion-sound velocity. We see from (25) that for $v_d>v_s$, $\gamma_{s0}<0$ and the interaction of ion-sound waves with the drifting electrons causes the wave amplitudes

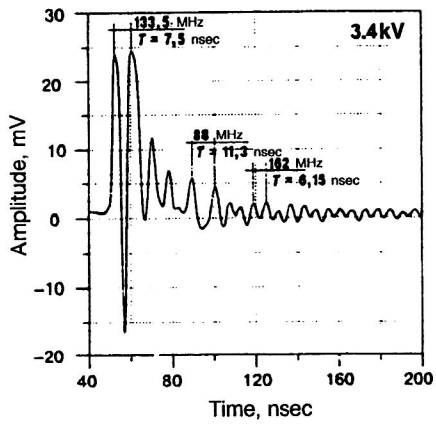

FIG. 18. Frequency of plasma oscillations of ions in the first and second avalanches and of ion sound for chamber filled with the gas mixture 80% CF_4+20% C_4H_{10}.

to grow. This growth will continue until nonlinear effects appear as a result of the interaction between the wave and the plasma particles. These interactions lead to exchange of energy between the oscillations and the particles, so that ultimately, when their final amplitude is reached, the growing waves change the plasma parameters. Under these conditions it is essential to take into account the nonlinear damping of the ion-sound oscillations.

It was shown in Ref. 53 that the main contribution to the function characterizing the nonlinear interaction of ion-sound waves with the plasma particles comes from the interaction between these waves and the ions. In the nonlinear interaction of two ion-sound waves with wave vectors $\mathbf{k}$ and $\mathbf{k}_1$, beats appear with phase velocity[53]

$$v_{\text{ph}}=\frac{v_s}{\sqrt{1+4kk_1(k-k_1)^2\sin^2\dfrac{\theta}{2}}}, \tag{26}$$

where θ is the angle between the vectors $\mathbf{k}$ and $\mathbf{k}_1$. If the interacting waves have close frequencies, so that $(k-k_1)/\sqrt{kk_1}\sim\sqrt{T_i/T_e}\sin\theta/2$, then the velocity v_{ph} is of the same order of magnitude as the ion thermal velocity v_i. These beats are strongly absorbed by ions, thereby leading to the damping of the original ion-sound waves and increase of the ion thermal energy. The increase of the ion temperature is also indicated by the oscillogram of Fig. 18, from which we see that the plasma oscillations of the ions become ion sound on the side of short wavelengths of frequency 162 MHz. For short-wavelength ion sound the limiting form of the dispersion equation (15) becomes (17), from which the ion temperature can be found. Taking the value of the adiabatic exponent for ions in (17) to be equal to that for heavy molecular gases, $\gamma=1.4$, we find the ion temperature:

$$T_+\sim\frac{\omega^2T_-M_+}{4\pi n_+e^2\gamma}\sim 0.2\ \text{eV};\quad k=\frac{2\pi}{\lambda};$$

$$\lambda=\left(\frac{\pi T_-}{n_+e^2}\right)^{1/2};\quad \omega=2\pi f. \tag{27}$$

The value of the ion temperature (more precisely, the average thermal energy) in the plasma regime is found to be roughly an order of magnitude higher than the temperature of the ions produced in the proportional regime (~0.025 eV).

The fact that the oscillations reach their final amplitude less than half a period after the start of the drift current through the chamber (Fig. 11b) indicates that the energy transfer from the drifting electrons to the wave has the nature of a phase resonance. In the voltage range 3.0–3.2 kV (Fig. 11b) an increase of the avalanche density does not cause the oscillation amplitude of the first two positive peaks, equal to 10 mV, to grow. The only change is in the duration of the tops of these peaks, which increases with increasing voltage and becomes comparable to the avalanche development time.

As noted above, the final amplitude reached by the wave in the buildup process is determined by the interaction of the wave with the plasma cloud, which causes the parameters of the latter to change. In the voltage range 3.0–3.2 kV these changes occur because the maximum delay of the cathode signal is established, during which intensive binding of the charges occurs and after which the drift current through the chamber begins. When nonlinear interactions between the wave and the particles are switched on, the ion temperature rises. However, first the change of parameters of the plasma cloud initiates the production of accelerated electrons in the avalanche, and then it initiates the development of a second avalanche, causing the amplitude to jump (see Figs. 7b and 10).

As the voltage is raised to 3.3 kV, a second series of more powerful oscillation buildup begins, which is accompanied by an increase of the current through the chamber, apparently due to multistage ionization. The behavior of the gas gain is also changed, so that it grows much more rapidly (Fig. 6). The average ion energy increases to 0.2 eV. A second series of plasma oscillations of the ions begins (Fig. 11c) in the second avalanche. The second buildup results in a final oscillation amplitude of 24 mV (Fig. 11c), which does not change up to a voltage of 3.8 kV.

The asymmetry of the oscillations in the first avalanche toward the positive phase is increased by a factor of 1.4 at the voltage 3.7 kV compared with the asymmetry at the voltage 3.5 kV (Fig. 11c). The amplitude and frequency characteristics of the ion oscillations in the second avalanche practically do not change in the range 3.5–3.8 kV. The frequency of the plasma oscillations of the ions in the second avalanche (Fig. 18) is 88 MHz and is apparently determined by the low electron energy.

According to plasma physics, when the final amplitude of the plasma oscillations is reached it is possible to excite a large number of waves in which an energy comparable to the thermal energy of the plasma is concentrated. Nonlinear effects due to the interaction between the waves and the plasma particles begin to be clearly manifested under these conditions. These effects are especially important for short-wavelength perturbations in the plasma, when the width of the leading front of the wave is comparable to the Debye radius. It therefore becomes necessary to include the dispersion of the ion plasma oscillations, which determines the wavelength dependence of the velocity at which the pertur-

bations propagate. The dependences of the perturbation propagation velocity on the amplitude and wavelength can cancel each other out, and the excitation of stationary waves in the plasma becomes possible.[53] Solitary and quasi-shock waves are the most important types of stationary wave arising in the propagation of a perturbation in a plasma. Depending on the conditions under which they are created, they can be either compression or rarefaction waves. As far as streamer formation is concerned, it is apparently favored by solitary compression waves, since the main feature of such waves is that the perturbations corresponding to them are not smeared out spatially with time, but preserve their form.[20,48]

It is quite clear that a streamer results from the intense processes occurring in the plasma cloud. The fact that it possesses a lifetime even when there is no external electric field[11] indicates that the streamer is a dense, quasineutral object with sufficient internal energy to exist independently. Therefore, it is very likely that a solitary compression wave is excited during its formation process.

Returning to plasma physics, we note that the interaction of excited waves with the plasma and with each other leads to irregular behavior of the electric fields arising in the plasma, and also to violation of the symmetry of the spatial distribution of the particle density. If the energy density in the plasma oscillations is sizable, the oscillations may be concentrated in a limited region of space and may be coupled.[48] As is well known, a stationary object of this type is called a soliton or a solitary wave.[20]

A solitary wave is a localized, self-sustaining wave packet. It represents a balance between two competing tendencies. On the one hand, the wave packet tends to spread owing to dispersion, because, according to the dispersion relation

$$\omega = v_{gr}\, k\left(1 - \frac{r_D^2 k^2}{2}\right), \tag{28}$$

shorter wavelengths move with lower velocity (v_{gr} is the group velocity of the wave). On the other hand, owing to nonlinearity, the wave packet is compressed, and so the dispersion effect is canceled.[48] It should be noted that the dispersion relation (28) was written down for plasma oscillations of ions.

The monograph of Ref. 53 gives a system of equations which can be used to study the density distributions of electrons $n_e(r,t)$, ions $n_i(r,t)$, and their velocities $v_e(r,t)$ and $v_i(r,t)$ in an electrostatic field with potential $\varphi(r,t)$ varying in space and time, and also to follow the development of nonlinear perturbations of finite amplitude. The propagation of nonlinear ion-sound waves has been studied in detail in Refs. 20 and 48 on the basis of the Korteweg–de Vries equation. Therefore, here we shall limit ourselves to the expressions relating the amplitudes of the electron and ion densities $n_{e\,\max}$ and $n_{i\,\max}$ to the maximum electrostatic potential of the solitary wave $\varphi_{\max}$ (Ref. 53):

$$n_{e\,\max} = n_{e0} \exp\left(\frac{e\varphi_{\max}}{T_e}\right),$$

$$n_{i\,\max} = n_{i0}\left(1 - \frac{2e\varphi_{\max}}{M_i V}\right)^{-1/2}, \tag{29}$$

where n_{e0} and n_{i0} are the electron and ion densities at the point $\varphi = 0$, and V is the velocity of a solitary wave, exceeding the velocity of the ion-sound waves. We see from (29) that $n_{e\,\max} > n_{e0}$ and $n_{i\,\max} > n_{i0}$, from which it follows that a solitary wave in a quasiequilibrium plasma with Maxwell distribution of the electron velocities is always a compression wave.

The maximum potential in the solitary wave $\varphi_{\max}$ and the propagation speed V are related as[48]

$$1 - e^{\psi} + 2\eta\left(1 - \sqrt{1 - \psi/\eta}\right) = 0, \tag{30}$$

where $\psi = e\varphi_{\max}/T_e$ and $\eta = M_i V^2/2T_e$. If the amplitude of the solitary wave is small ($e\varphi_{\max} \ll T_e$), its propagation velocity tends to the phase velocity of the ion-sound wave $V = \sqrt{T_e/M_i}$. Otherwise, the maximum amplitude will be

$$e\varphi_{\max} = 1.3T_e, \quad V = 1.6\sqrt{T_e/M_i}. \tag{31}$$

The oscillograms of Figs. 11b and 11c illustrate the fact that, owing to the development of instabilities leading to nonlinear phenomena in the plasma, the plasma cloud actually undergoes a gradual compression. As the density of the plasma cloud increases the asymmetry of the oscillations toward the positive phase also grows, which indicates an increase of the binding electrostatic force and enhancement of the collective effect, i.e., the ions carry the electrons along in the oscillation process. The combined motion of the unlike charges induced by the oscillating ions tends to extend the saturation of positive amplitudes and leads to the appearance of elastic (sound) oscillations. Comparing the oscillograms of Figs. 11b and 11c, we see that in the voltage range 3.0–3.2 kV, where a final amplitude of 10 mV is reached, the behavior of the plasma oscillations is considerably different from that of the plasma oscillations measured in the range 3.3–3.7 kV. A final amplitude of 24 mV is reached in the last range as a result of the second stage of oscillation buildup. Whereas in the first range the nonlinear effects are still very small and the damping of the plasma waves is proportional to the small parameter[20] $\sqrt{m_e/M_i}$, in the second range the picture is changed dramatically, owing to the increasingly important role of nonlinear effects. It is observed that not only does the duration of the ion plasma oscillations decrease, but also the amplitude of these oscillations is significantly weakened after the first period of oscillations. For this to occur it is necessary that the perturbation of the particle density δn_e in the plasma cloud satisfy the condition[53] $\delta n_e/n_e \gg \sqrt{m_e/M_i}$.

Unfortunately, owing to the presence of electrically negative impurities in the CF_4 gas (cf. Figs. 11a–11e), at the working voltages it is not possible to reach the critical charge density in the avalanche and move the chamber into the self-quenching streamer regime in order to follow the streamer formation to its final stage. However, on the basis of the data given above, it can be assumed that gradually, during the compression process, a dense object representing the nucleus of a streamer is formed from the bulk of the quasineutral ensemble of charged particles as its density increases.

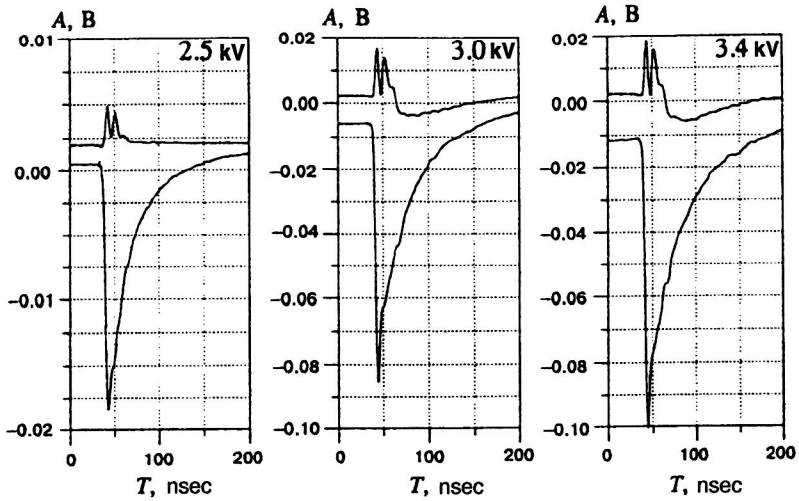

FIG. 19. Oscillograms of signals averaged over 256 events from the control wires (upper figures) and from the anode for chamber filled with the gas mixture 80% CF_4+20% C_4H_{10}+2.5×10^{-4} Hg. The chamber voltage is given on the oscillograms.

To check these assumptions, streamer formation was studied by using the gas mixture 80% CF_4+20% C_4H_{10}+2.5×10^{-4} Hg. Mercury vapor was added because of the large cross section for the ionization of atoms by metastable molecules, and also the presence of associative ionization involving two excited atoms,[21] $Hg(6^3P_1)+Hg(6^3P_0)\rightarrow Hg_2^+ + e$. The inclusion of these processes in the electron avalanche tends to increase its density, as indicated by the oscillograms shown in Figs. 19 and 20. The oscillograms in Fig. 19 were obtained by averaging 256 events. The oscillograms for single events at a fixed chamber voltage of 2.6 kV are given in Fig. 20. In the oscillogram (Fig. 19) obtained for chamber voltage 2.5 kV we see only the positive phase of the ion plasma oscillations, which extend for one period. Ion-sound oscillations are absent, owing to the intense nonlinear effects in the plasma cloud. Sound oscillations begin to be weakly manifested as the chamber voltage is decreased. This behavior of the avalanche is related to the fact that the range of the plasma regime is strongly limited by the rapid growth of the density of the plasma cloud and nonlinear processes, because it approaches the streamer regime earlier and more and more quickly. In the oscillograms obtained for chamber voltages of 3.0 and 3.4 kV we clearly see the features of the production and the profile of the solitary wave propagating toward the cathode, because the compression of the plasma cloud is due to longitudinal oscillations of the ions. Since the electrostatic potential of a solitary compression wave is always positive, the signals induced by it at the control wires and at the anode as the wave moves toward the cathode will have the opposite polarity.

Comparing the oscillograms in Fig. 19, we see that the time at which the solitary wave appears is shifted to the left as the voltage increases. The amplitude of the anode signal practically does not change, owing to the strong saturation associated with the increase of the electric field of the volume charge up to the strength of the external field. The duration of the anode signal corresponds to the duration of the signal formed in the self-quenching streamer regime,[35] and is more than five times greater than the duration of the signal formed in the plasma regime.

The oscillograms of the single signals shown in Fig. 20 are more informative. The first oscillogram illustrates the excitation and rapid damping of a solitary wave with low potential inside the streamer. Information about this is contained in the anode signal and is manifested in the change of its trailing edge, induced by the superposition on it of the

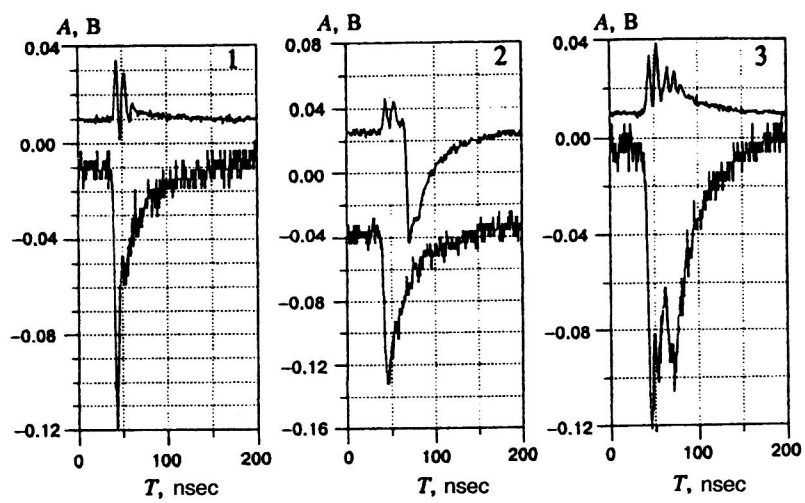

FIG. 20. Oscillograms of signals from the control wires (upper figures) and from the anode for chamber filled with the gas mixture 80% CF_4+20% C_4H_{10}+2.5×10^{-4} Hg. The chamber voltage is 2.5 kV.

induced signal from the solitary wave moving inside the streamer toward the cathode.

The ions play the leading role in the damping of a solitary wave inside a streamer, because their average thermal velocity is practically comparable to the propagation velocity of the solitary wave. According to (31), the amplitude and velocity of the solitary wave are restricted, because solitary waves formed in the streamer closer to the anode will be damped out. If a wave is formed in the streamer closer to the cathode, when its potential is sufficiently high it can leave the streamer. This is the situation illustrated in the second oscillogram of Fig. 20. In this oscillogram we clearly see the profile of the solitary wave. The time characteristics of the anode signal exactly mimic the profile of the solitary wave. The amplitude of the signals induced at the control wires by the solitary wave leaving the streamer varies in a very wide range and sometimes nearly reaches the amplitude of the anode signal. As the amplitude increases the wave is squeezed and the size of the region occupied by the perturbation is inversely proportional to the square root of the amplitude of the solitary wave.[48]

The third oscillogram illustrates the formation of two streamers. Two groups of plasma oscillations with strong asymmetry in the region of the positive phase are clearly distinguished in the upper oscillogram. The magnitude of the asymmetry of the second group of plasma oscillations relative to the equilibrium position is higher than for the first group. This apparently indicates that the density of the second streamer is slightly larger than that of the first. Solitary waves indicating streamer formation are damped in them, but information about their motion is clearly seen in the lower oscillogram of the anode signal. Moving to the upper oscillogram the time points at which the maximum amplitudes of the signals induced by solitary waves at the anode are reached, we obtain the approximate time needed to reach the critical density in each plasma cloud. We see from this figure that this density is reached after completion of the avalanche over a period of the plasma oscillations, i.e., after about 7.5 nsec.

However, the most important, third oscillogram apparently reflects the mechanism of secondary-electron production at the front of the first streamer. Since the field inside the streamer is practically zero, while the potential of the first solitary wave is higher than the average electron energy (31), the wave can pull some of the electrons along with it. In moving with acceleration to the region of stronger field at the front of the streamer, the electrons can accumulate a large energy in their directional motion and leave the streamer. Let us estimate the number of such electrons. We shall assume that the streamer volume is equal to half the avalanche volume, estimated in Sec. 8.3, i.e., 0.75×10^{-6} cm^3, and the number of electrons in it is 10^8. If the width of the wave front is equal to the Debye radius, i.e., 1.8×10^{-4} cm, and it is formed at a distance of 2×10^{-3} cm from the front of the streamer, then a volume $1.8\times10^{-4}\times1.8\times10^{-4}\times2\times10^{-3}=6.5\times10^{-11}$ cm^3 will contain approximately 8×10^3 electrons. Therefore, even if the wave pulls along 1% of these electrons over 10–20 electron mean free paths to the region of strong total field, then, in drifting to the front of the streamer, these electrons will be able to generate a powerful avalanche. A succession of such processes in the total field ensures the continuous propagation of the streamer toward the cathode. Since the motion occurs in a nonuniform field, the streamer stops growing, owing to the falloff of the total field as soon as the electron current from the last avalanche is insufficient to support the quasineutrality of the streamer. This causes it to decay.

Our analysis of the experimental data allows us to answer the following questions.

1. What is an anode-directed streamer?
2. Does the streamer come into contact with the anode?
3. Why is the dead time of a multiwire chamber operating in the self-quenching streamer regime so long?

1. According to the data given above, and also the data from Refs. 46 and 47, streamer formation requires 10–30 nsec, depending on the conditions. The streamer is formed after completion of the avalanche, the stages of which are clearly seen in oscillograms. As far as an anode-directed streamer[11] is concerned, the data obtained give no indication that one is formed. The avalanche development time at gains corresponding to the start of streamer formation is very small and equal to 4.5 nsec. During this time in the direction toward the anode only accelerated electrons are produced, and these reach the anode in a fraction of a nanosecond, owing to the large drift velocity. There are thus no grounds for speaking of transformation of an avalanche into an anode-directed streamer in a wire chamber.

The effective ionization produced by the rather large number of electrons which undergo constant acceleration without bremsstrahlung apparently generates a very dense avalanche in a small solid angle, which rapidly grows toward the anode and therefore creates the impression of a streamer.

2. Using the expression for the conductivity in a weakly ionized plasma,[21] $\sigma\sim10^{-16}n_e/P[\text{atm}]\Omega^{-1}$ cm^{-1}, let us estimate its value for our case. For gas pressure in the chamber $P=1$ atm and $n_e=2\times10^{13}$ cm^{-3}, we have $\sigma=2.1\times10^{-3}\Omega^{-1}$cm^{-1}. It then follows that the presence of plasma and ion-sound oscillations in the streamer indicate that it does not come into contact with the anode. Otherwise, if the streamer came into contact with the anode, the electrons inside the streamer would reach the anode in 1–2 nsec, owing to the high conductivity of the plasma, and the oscillations would stop. According to the oscillograms of Fig. 11c, there are oscillations not only in the first avalanche, where the streamer is formed, but also in the second series of plasma oscillations which are transformed into prolonged ion-sound oscillations.

3. In chambers operating in the self-quenching streamer regime, a segment of the signal wire "dies" after the passage of a particle. The effective value of the product of the length of this segment and the time during which it is insensitive is 33 μsec·cm (Ref. 35). This is related to the fact that, after the second avalanche occurs, the streamer is blocked between the ion cloud created by the fast electrons and the anode, and the quasineutral ion cloud of the second avalanche. Ambipolar diffusion and ambipolar drift of the charged particles of the streamer toward the cathode will be possible only after most of the ion cloud of the second ava-

lanche has spread out. The dead time of the chamber will therefore be determined mainly by the streamer lifetime. The effective drift velocity of the ions in the streamer will be strongly suppressed, owing to their high mobility.

This time can be estimated in two ways. In the first, it is the time needed for the streamer to move beyond the confines of the avalanche-production region, determined by the speed of motion of the ambipolar flux (12) and the ion distribution in the streamer. The second way is to use the decrease of the charge density in the streamer due to electron recombination according to the expression[21]

$$\frac{dn_e}{dt}=-\beta n_e n_+, \quad n_e=\frac{n_e^0}{1+\beta n_e^0 t_{\text{rec}}}\to\frac{1}{\beta t_{\text{rec}}}. \tag{32}$$

As an example, since the value of the electron–ion recombination coefficient for CF_4 is not known, we can use the recombination coefficient β for inert gases, the value of which for a plasma with electron temperature 0.2 eV lies in the range $(0.2–0.3)\times10^{-7}$ cm^3/sec. For $n_e=2\times10^{13}$ cm^{-3} the recombination time (or the streamer decay time) will be 17–25 μsec. Since the recombination coefficient is somewhat smaller in a molecular plasma than in an atomic plasma, the estimate is in good agreement with experiment.

9. POSSIBLE APPLICATIONS OF THE PLASMA REGIME

On the basis of the above results, we can single out some of the main features manifested in the transformation of an electron avalanche into a plasma which can be used for practical applications.

1. It was mentioned in Sec. 8.3 that when the γ source ^{55}Fe is used, the ion plasma oscillations begin about 300 V earlier than when a β source is used. This is because the required avalanche density for the transition to the plasma state is reached for lower gain in the chamber, owing to the large ionizing power of the γ source. The sensitivity of plasma and ion-sound oscillations of the ions to the ionization can be used to identify relativistic charged particles. Basically, this method is analogous to that of measuring the primary ionization, which, as is well known, has a number of advantages over measurement of the total ionization. Moreover, our method is much simpler than the primary-ionization method proposed by Walenta,[49] because the oscillations are counted in ordinary narrow-gap chambers. In Fig. 11b we see that for a gain of $\geqslant5\times10^6$ (chamber voltage 3.0–3.2 kV) the amplitudes of the positive oscillation phase measured directly from the anode wires located to the left and to the right of the triggered wire lie in the range 1–15 mV for a load of 50 Ω, while the observed number of oscillations is ~25, roughly the same as the number of clusters formed in the gas over a length of 4 mm. For these gains, a narrow-gap chamber with signal-electrode spacing equal to 2 mm can operate in beams of density $5\times10^5–10^6$ sec^{-1} cm^{-2}. A MAR8 high-frequency solid-state amplifier can be used to amplify the signals.[27] The electronic channel must contain an amplifier, a comparator, and an eight-bit counting element operating at 200 MHz. Electronics of this design will allow improvement of the determination of the particle coordinates by a factor of two when using the number of recorded oscillations in the channels to the left and to the right of the triggered wire.

Therefore, when the number of oscillations in one gap of the chamber is $N_{\text{ch}}(1)=25$, it is possible to make an identifier containing 40 layers of narrow-gap chambers (or standard chambers with a thick anode wire) with a resolution of $\sigma_{\text{ch}}/N_{\text{ch}}(40)\approx3\%$, where $N_{\text{ch}}(40)$ is the average number of recorded oscillations in the 40 layers, and σ_{ch} is the rms deviation of the distribution $N_{\text{ch}}(40)$. This resolution ensures the reliable identification of (π,k,p) particles in the momentum range 5–30 GeV/c. The proposed identifier based on narrow-gap chambers will have a length of up to 25–30 cm, which is 15 times shorter than the identifier based on measurement of the primary ionization,[50] and 50 times shorter than an identifier measuring the total ionization losses of the particles.[51,52]

2. Owing to its basic characteristics, the use of the plasma regime in physics experiments offers wide-ranging possibilities. For clarity, let us list these characteristics together with those of the self-quenching streamer regime[7] (given in parentheses).

- Signal amplitude $A=0.2-4$ mA ($A=0.2-4$ mA).
- Stability of operation or width of the counting characteristic 1400 V (1000 V).
- Amplitude spread $\Delta A/A\sim15\%$ ($\Delta A/A\sim40\%$).
- Duration of the signal at half-max $t_{1/2}\sim5$ nsec ($t_{1/2}\sim40$ nsec).
- Duration of the signal at 10% of the maximum amplitude $t_{0.1}\sim10$ nsec ($t_{0.1}\sim100$ nsec).
- Counting rate 10^5 sec^{-1} cm^{-2} (10^3 sec^{-1} cm^{-2}).
- Radiation stability 5 C/cm (0.5 C/cm).

Clearly, significantly better parameters are obtained in the plasma regime, and so it can be used successfully in hadron calorimeters and muon identifiers instead of the self-quenching streamer regime used at present.

Owing to the high counting rate and the small amplitude spread in the chambers, it is easy to realize an efficient and fast trigger using the multiplicity of recorded particles at the analog level. The electron avalanches produced at the anode wires create at the cathode a total induced charge of $n\Delta q$ (n is the number of avalanches, and Δq is the charge induced at the cathode by an anode avalanche). The total signal is sent to the discriminator and, if it exceeds the preset threshold, triggers it.

Narrow-gap chambers operating in the plasma regime can be used to measure the number of particles in an avalanche and the particle spatial distribution in a compact and fast electromagnetic calorimeter.[28]

3. Since the ions and electrons of the avalanche drift in opposite directions in the chamber, when ambipolar diffusion comes into play the particle drift velocity will fall. The time when deceleration forces begin to act can be determined from the appearance of a delay in the formation of the signal at the cathode. The use of this technique allows optimization of a fast gas mixture for a wide range of values of the reduced electric-field strength E/p in wire chambers operating at large loads. The gas composition is optimized by eliminating delay of the cathode signal by using quench additives in

the working volume of the chamber at high voltage.

4. The ion component oscillates in the self-consistent electric field of the electron component. Therefore, if the frequency of the ion oscillations is measured before the oscillation amplitude reaches saturation, it is possible to estimate the average electron energy. The possibility of making such estimates is especially important for molecular gases in modeling and calculating the physical processes occurring in an avalanche. Since ion plasma oscillations are transformed into ion-sound oscillations of short wavelength, the frequency of these oscillations determines the average ion energy at the time when the ion oscillations are transformed into ion sound. Knowledge of the ion temperature in the streamer allows fairly accurate calculation of its internal energy.

An approximate estimate of the avalanche size can be obtained by using the density of charge carriers, which is determined from the frequency of the ion plasma oscillations.

5. It is clear from Figs. 11a–11c that the spatial distribution of the charged particles of the plasma is stable to small shifts during the time needed for streamer formation. As the current through the chamber grows, the small oscillations grow and ultimately reach amplitudes at which the plasma parameters are changed. It was noted in Sec. 8.4 that two stages of buildup of ion oscillations are realized in the gas mixture 80% CF_4+20% C_4H_{10}. Owing to these processes, an ever greater amount of energy is concentrated in the ion oscillations, which can affect the processes tending to establish equilibrium and the averaged characteristics of the plasma.[48] Accordingly, it is interesting to select a gas mixture for which it is possible to obtain a large number of oscillation-buildup stages. These processes must result in the formation of a very dense streamer, at whose head the electric field must be comparable to the field at the anode wire. The basis for this is the different manifestation of the plasma oscillations in different gas mixtures. It follows that the plasma parameters can be controlled by the appropriate choice of quenching, polar, and electrically negative additions.

10. CONCLUSION

In summarizing our experimental study of avalanche development in wire chambers, it can be stated that:

- When the chamber operates in the regime of large gas gain, the electron avalanche is transformed into production of a plasma with the basic properties characteristic of a plasma.
- The use of plasma physics allows explanation of not only the conditions for streamer formation and growth toward the cathode, but also the individual elementary processes and their effects on and interactions with each other in gas discharge.
- The new approach to the study of gas discharge is fruitful both for studying the actual mechanism of gas discharge, and for technical applications of this phenomenon.

The analysis of the experimental data using the new approach shows that the stages of avalanche development can be represented as follows.

1. The Coulomb forces, which tend to bind charges of opposite signs, begin to play a role at low avalanche density, when the number of charge carriers in the avalanche reaches $\sim 5\times 10^5$.

2. As the avalanche density increases, the charge-binding mechanism becomes more important, and the spatial scales of the charge separation decrease. Consequently, the ions and electrons cannot be separated from each other. This means that while the binding forces act there is no drift current through the chamber, and the signals at the anodes are formed owing to the diffusion current induced by the presence of gradients in the avalanche.

3. When the gain in the chamber is $\geqslant 10^6$, the electric field of the charge separation is such that there is no current through the chamber while the avalanche develops. During this time, the space charge of the avalanche is effectively neutralized by bremsstrahlung and the binding of slow electrons, and at the same time the conditions are created for the electrons located at the front of the avalanche to enter the regime of continuous acceleration.

4. As the avalanche density grows, perturbations induced by the charge separation or by macroscopic movements of charges do not remain localized. Owing to the long-range Coulomb interactions, they lead to small plasma oscillations of the ions and propagate in the form of a wave along the entire avalanche. The duration of the oscillations grows as a function of the primary ionization density and the density and composition of the working gas.

5. As a result of energy transfer to the electrons by plasma waves, the oscillations build up successively, and their amplitude reaches saturation. The interaction between the oscillations of the plasma cloud and the plasma cloud itself leads to a change of its state, owing to the change of the plasma parameters. This is primarily expressed as an increase of the ion temperature.

6. The interaction of intense nonlinear waves with each other and with the plasma cloud leads to the formation of a dense, quasi-neutral bunch with finite lifetime, called a streamer. The perturbation arising from violation of the symmetry of the spatial distribution of the particle density in the plasma cloud is manifested in the formation of a solitary wave whose electrostatic potential determines the size of the region occupied by the density perturbation.

7. Since the electric field inside the streamer is close to zero, if the potential of the solidary wave is higher than the average electron energy, the wave can pull some of the electrons along toward the cathode. In moving with acceleration to the region of stronger field at the head of the streamer, the electrons can accumulate a large amount of energy in directional motion and leave the streamer to reach the region of weaker field. In drifting to the region of strong field ahead of the streamer front, where the field is the sum of the external field and the ion field, the electrons begin a new avalanche-formation process. As a result of the self-sustaining mechanism ensuring secondary electrons from the avalanche, the discharge begins to resemble a streamer growing toward the cathode.

8. No indications of the formation of an anode-directed streamer during the avalanche-development time were found in the measurements. During this time, electrons undergoing constant acceleration appear on a finite segment of the avalanche-production region and move to the anode with velocity roughly three to four times greater than the drift velocity of the slow electrons in the avalanche.

9. A perturbation induced by violation of the spatial distribution of the particle density will propagate in opposite directions.[20] Therefore, in uniform fields, when a streamer is formed far from the anode, the cause of rapid electron production ahead of the avalanche might be a solitary wave. It can pull electrons along as it propagates toward the anode. In their accelerated motion to the region of strong field at the front of the avalanche, the electrons can accumulate a large amount of energy in their directional motion.

10. The different behavior of the ion plasma oscillations in different gas mixtures indicates that it is possible to control the plasma parameters in an avalanche by using quenching or electrically neutral admixtures.

11. The dead time of a wire chamber operating in the self-quenching streamer regime is determined by the streamer lifetime, which depends on the intensity of electron–ion recombination in the working gas that is used.

12. In operation in the self-quenching streamer regime with a gas mixture containing an inert gas, the processes preceding streamer formation will actually occur during the avalanche development time, which ensures very rapid growth of the streamer toward the cathode.

13. Use of the plasma (prestreamer) regime instead of the self-quenching streamer regime is preferable in practice, because for the same current characteristics the former has much smaller dead time, higher radiation stability, and better time resolution.

In concluding this study, it should be particularly emphasized that we have primarily tried to display experimental results which reflect the complexity and diversity of the processes occurring in an electron avalanche. The use of CF_4 containing electrically negative admixtures as the main working gas allowed extension of the region of transformation of an electron avalanche into a streamer to high voltage, and made it possible to observe the dynamics of the processes leading to this transition in a "slower" form by using control wires (probes). The dynamics is certainly very complicated, particularly in the streamer-formation region, where there is a large gap in our knowledge. Therefore, we do not claim that the present study is complete or represents an accurate interpretation of the large amount of experimental data which have been obtained so far. It is impossible to do this in a single study, even in a large one, because the complexity and importance of the problem require many experiments, calculations, and modelings in order to arrive at any conclusion. And ultimately the main conclusion following from the present study is that information about gas discharge can be obtained not from individual elementary processes, but only from the dynamics of its development.

The author considers it his pleasant duty to sincerely thank Corresponding Member of the Russian Academy of Sciences V. P. Dzhelepov, Corresponding Member of the Russian Academy of Sciences I. N. Meshkov, Professor Yu. K. Akimov, Professor V. G. Zinov, Professor V. I. Komarov, Professor A. A. Tyapkin, and Professor V. B. Flyagin for valuable comments and advice, and also for their interest in and support of this study.

The author is deeply grateful to A. Yu. Petrus and I. N. Potrap for useful discussions, unflagging interest, and help in performing the measurements and preparing this article.

Finally, the author takes this opportunity to sincerely thank his colleague at the Paul Scherer Institute, Dr. D. Eger, for his great interest in and useful discussions about the problems involving wire chambers operating in the regime of large gas gain.

[1] R. Bonclier, G. Charpak, Z. Dimčoviski *et al.*, Nucl. Instrum. Methods **88**, 149 (1970).
[2] S. Brehin, A. Diamant Berger, G. Marel *et al.*, Nucl. Instrum. Methods **123**, 225 (1975).
[3] G. D. Alekseev, V. V. Kruglov, and D. M. Khasins, Nucl. Instrum. Methods **153**, 157 (1978).
[4] G. D. Alekseev, V. V. Kruglov, and D. M. Khazins, Preprint R13-80-653, JINR, Dubna (1980) [in Russian].
[5] A. I. Abramov, Yu. A. Kazanskiĭ, and E. S. Matusevich, *Foundations of Experimental Methods in Nuclear Physics* [in Russian] (Atomizdat, Moscow, 1970).
[6] *Electrical Breakdown of Gases*, edited by J. M. Meek and J. D. Craggs (Wiley, New York, 1978) [Russ. transl., IL, Moscow, 1980].
[7] D. M. Khazins, Doctoral Dissertation, Dubna (1985) [in Russian].
[8] H. Raether, Z. Phys. **110**, 611 (1938).
[9] A. Przybylsky, Z. Phys. **151**, 264 (1958).
[10] T. H. Teich, Z. Phys. **199**, 378 (1967).
[11] H. Raether, *Electron Avalanches and Breakdown in Gases* (Butterworths, London, 1964) [Russ. transl., Mir, Moscow, 1968].
[12] G. D. Alekseev, V. V. Kruglov, and D. M. Khazins, Preprint D13-12027, JINR, Dubna (1978) [in Russian].
[13] H. Kalmar, E. V. Komissarov, V. S. Kurbatov *et al.*, in *Proceedings of the Third Workshop on Physics of UNK*, Protvino, 1990, p. 31.
[14] É. D. Lozanskiĭ and O. B. Firsov, *Spark Theory* [in Russian] (Atomizdat, Moscow, 1964).
[15] B. M. Smirnov, *Atomic Collisions and Elementary Processes in a Plasma* [in Russian] (Atomizdat, Moscow, 1964).
[16] G. Francis, *Ionization Phenomena in Gases* (Butterworths, London, 1960) [Russ. transl., Atomizdat, Moscow, 1964].
[17] D. A. Frank-Kamenetskiĭ, *Lectures on Plasma Physics* [in Russian] (Atomizdat, Moscow, 1964).
[18] O. A. Omarov, A. A. Rukhadze, and G. A. Shneerson, Zh. Tekh. Fiz. **49**, No. 9, (1997) [*sic*].
[19] A. A. Aleksandrov, A. S. Bogdankevich, and A. A. Rukhadze, *Foundations of Plasma Electrodynamics* [in Russian] (Vysshaya Shkola, Moscow, 1988).
[20] E. M. Lifshits and A. P. Pitaevskiĭ, *Physical Kinetics* [in Russian] (Nauka, Moscow, 1979).
[21] Yu. P. Raĭzer, *The Physics of Gas Discharge* [in Russian] (Nauka, Moscow, 1992).
[22] A. von Engel, *Ionized Gases*, 2nd ed. (Clarendon Press, Oxford, 1965) [Russ. transl. of 1st ed., Fizmatgiz, Moscow, 1959].
[23] E. M. Gushchin, E. V. Komissarov, Yu. V. Musienko *et al.*, Nucl. Instrum. Methods Phys. Res. A **351**, 345 (1994).
[24] G. D. Alekseev, V. V. Kruglov, and D. M. Kazins, in *Proceedings of the Third Intern. Meeting on Proportional and Drift Chambers* [in Russian], D13-11807, JINR, Dubna (1978).
[25] Gold-plated tungsten alloy wires type 861, No. 60 finish made by Luma Lampan AB, Kalmar, Sweden; Distributor: SAES Getters/USA, Inc.
[26] H. Kalmar, A. G. Ketikjan, E. V. Komissarov *et al.*, Nucl. Instrum. Methods Phys. Res. A **307**, 279 (1991).
[27] Industrial Electronics, GMBH. em Mini-Circuits Catalog.
[28] S. Majewski, G. Charpak, A. Breskin, and G. Mikenberg, Nucl. Instrum. Methods Phys. Res. **217**, 265 (1983).

[29] K. Genser and R. Walczak, Nucl. Instrum. Methods Phys. Res. A **253**, 264 (1984).
[30] R. Henderson, IEEE Trans. Nucl. Sci. **NS-34**, 528 (1987); **NS-35**, 477 (1988).
[31] L. L. Kurchaninov, Preprint 89-131, IHEP, Serpukhov (1989) [in Russian].
[32] J. Fischer, A. Hrisoho, V. Radeka, and P. Rehak, Nucl. Instrum. Methods Phys. Res. A **238**, 249 (1985).
[33] A. Oed, Nucl. Instrum. Methods Phys. Res. A **263**, 351 (1988).
[34] Y. Y. Lachin, L. V. Miassoedov, I. V. Morozov *et al.*, Nucl. Instrum. Methods Phys. Res. A **361**, 77 (1995).
[35] G. D. Alekseev, V. V. Kruglov, and D. M. Khazins, Fiz. Élem. Chastits At. Yadra **13**, 703 (1982) [Sov. J. Part. Nucl. **13**, 293 (1982)].
[36] E. E. Kunhardt and W. W. Byszewski, Phys. Rev. A **21**, 2069 (1980).
[37] A. I. Pavlovskiĭ, L. P. Babich, T. V. Loĭko, and L. V. Tarasov, Dokl. Akad. Nauk SSSR **281**, 1359 (1985) [Sov. Phys. Dokl. **30**, 303 (1985)].
[38] Yu. D. Korolev and G. A. Mesyats, *The Physics of Voltage Breakdown of Gases* [in Russian] (Nauka, Moscow, 1991).
[39] V. K. Lyapidevskiĭ, *Methods of Radiation Detection* [in Russian] (Énergoatomizdat, Moscow, 1987).
[40] S. C. Brown, *Basic Data of Plasma Physics* (MIT Press, Cambridge, Mass., 1959) [Russ. transl., Atomizdat, Moscow, 1978].
[41] D. A. Frank-Kamenetskiĭ, *Plasma: the Fourth State of Matter* (Plenum Press, New York, 1972) [Russ. original, Atomizdat, Moscow, 1963].
[42] M. Mitchner and C. H. Kruger, Jr., *Partially Ionized Gases* (Wiley, New York, 1973) [Russ. transl., Mir, Moscow, 1976].
[43] B. N. Shvylkin, *Problems in Gas Electronics and Plasma Physics* [in Russian] (Nauka, Moscow, 1978).
[44] K. Yamamoto and N. Ikuta, J. Phys. Soc. Jpn. **63**, 2157 (1994).
[45] N. S. Rudenko and V. I. Smetanin, Izv. Vyssh. Uchebn. Zaved. Fiz. **7**, 34 (1977).
[46] H. Toll, in *Electron Avalanches and Breakdown in Gases*, H. Raether (Butterworths, London, 1964) [Russ. transl., Mir, Moscow, 1968].
[47] K. Wagner, in *Electron Avalanches and Breakdown in Gases*, H. Raether (Butterworths, London, 1964) [Russ. transl., Mir, Moscow, 1968].
[48] B. M. Smirnov, *Physics of Weakly Ionized Gases: Problems With Solutions* [in Russian] (Nauka, Moscow, 1985).
[49] A. H. Walenta, Phys. Scr. **23**, 354 (1981).
[50] Yu. A. Budagov, V. Glinka, F. P. Nagaĭtsev *et al.*, Preprint 13-84-337, JINR, Dubna (1984) [in Russian].
[51] W. W. M. Allison, C. B. Brooks, L. Lyons *et al.*, Nucl. Instrum. Methods **163**, 331 (1979).
[52] V. Baruzzi, R. Carosio, F. Crijns *et al.*, Nucl. Instrum. Methods Phys. Res. **207**, 339 (1983).
[53] A. I. Akhiezer, I. A. Akhiezer, R. V. Polovin *et al.*, *Plasma Electrodynamics* [in Russian] (Nauka, Moscow, 1974).

Translated by Patricia A. Millard